Desalination

Dynamic Modelling of a Multi-Effect Vertical Falling-Film Evaporator for Water Reuse in CSP Plants

--Manuscript Draft--

Manuscript Number:	
Article Type:	Full Length Article
Section/Category:	Thermal desalination processes
Keywords:	Dynamic model; Multi-effect Evaporation; Vertical Falling-film; Dymola; Sensitivity analysis
Corresponding Author:	Bartolomé Ortega-Delgado, Ph.D. Centro de Investigaciones Energeticas Medioambientales y Tecnologicas Departamento de Energia Tabernas, Almería SPAIN
First Author:	Bartolomé Ortega-Delgado, Ph.D.
Order of Authors:	Bartolomé Ortega-Delgado, Ph.D.
	Patricia Palenzuela, Ph.D.
	Javier Bonilla, Ph.D.
	Manuel Berenguel, Ph.D.
	Lidia Roca, Ph.D.
	Diego-César Alarcón-Padilla, Ph.D.
Abstract:	This work presents the dynamic modeling of a vertical multi-effect evaporator plant designed and manufactured for its installation at a commercial concentrating solar power (CSP) plant, within the framework of EU H2020 project SOLWARIS (Solving Water Issues for CSP plants). The model has been developed using Modelica computational language and implemented in Dymola software environment. The results from the validation show a good agreement against the design data, obtaining relative errors lower than 5%. The dynamic response of the plant against external disturbances of the motive steam mass flow rate, feedwater mass flow rate and condenser pressure has been investigated. The main results reveal that increasing the motive steam flow rate by 5% produces a similar increment of the water recovered (5.2%), although the concentrate salinity is raised to an unsafe operation zone (106%) that could lead to scaling issues in the evaporators. The same effect occurs when the feedwater is decreased by 5% from its nominal value, causing a significant rise in the concentrate salinity (163%). In those cases, the simultaneous and proportional variation of the motive steam and feedwater mass flow rates allows maintaining the outlet concentrate salinity far from scale formation limits.
Suggested Reviewers:	Andrea Cipollina, Ph.D. Associate Professor, Università degli Studi di Palermo: Universita degli Studi di Palermo andrea.cipollina@unipa.it Dr. Cipollina has extensive expertise in modelling multi-stage flash and multi-effect distillation processes, along with membrane desalination processes
	Ali Altaee, Ph.D. Associate Professor, University of Technology Sydney alialtaee@hotmail.com Dr. Ali Altaee is working at the forefront of renewable energy, water engineering, and soil remediation, developing innovative technologies in alternative water sources.
	Marios Georgiou, Ph.D. Head of PROTEAS Operations Facility, The Cyprus Institute m.c.georgiou@cyi.ac.cy Dr. Georgiou is a core member of the Energy and Renewables Group for the last 8 years. His mainly focus is the implementation of the CSP – DSW project (Concentrated

	Solar Power for Cogeneration of Electricity and Desalination of Sea Water) both from the scientific prospective so as from the operational and maintenance.
Opposed Reviewers:	

Almería 25 October 2021

Editor
Desalination

Dear Editor,

Attached you can find the manuscript:

"Dynamic Modelling of a Multi-Effect Vertical Falling-Film Evaporator for Water Reuse in CSP Plants"

written by Dr. Bartolomé Ortega-Delgado, Dr. Patricia Palenzuela, Dr. Javier Bonilla, Dr. Manuel Berenguel, Dr. Lidia Roca and Dr. Diego-César Alarcón-Padilla.

The work presented in this manuscript has been carried out within the framework of the EU H2020 SOLWARIS project, aiming at reducing the water consumption in CSP plants. The manuscript thoroughly describes the dynamic modeling of a vertical multieffect evaporation plant and its implementation in Modelica programming language. Thus, we believe it can be a nice contribution to the literature relevant to dynamic modeling of vertical MEE plants.

Please, consider the manuscript for possible publication in Desalination.

I look forward to hearing from you soon,

Kind regards

Bartolomé Ortega

Researcher
Solar Thermal Applications Unit
Plataforma Solar de Almería,
Carretera de Senés km. 4; P.O.BOX 22, 04200 Tabernas (Almería), Spain
Phone: (+34) 950 387800 Ext. 973, Fax: (+34) 950 365015
Email: bartolome.ortega@psa.es
URL: www.psa.es

Highlights

1. A dynamic model for a vertical multi-effect evaporator plant is developed
2. The model is aimed at water recovery in concentrating solar power plants
3. The model is validated with good agreement against data provided by manufacturer
4. Transient response against disturbances on the operational inputs is investigated
5. Joint increment of motive and feed flow rates by 5% boosts water recovery by 4.2%

Dynamic Modelling of a Multi-Effect Vertical Falling-Film Evaporator for Water Reuse in CSP Plants

Bartolomé Ortega-Delgado[1,*], Patricia Palenzuela[1], Javier Bonilla[1], Manuel Berenguel[2], Lidia Roca[1], Diego-César Alarcón-Padilla[1]

[1]CIEMAT-Plataforma Solar de Almería-CIESOL. Ctra.de Senés s/n, 04200 Tabernas, Almería, Spain

[2] Department of Informatics, CIESOL-ceiA3, University of Almeria, Ctra. Sacramento s/n, 04120 Almería

[*]Corresponding author, bartolome.ortega@psa.es, Tel.: +34 950 387800. Ext. 973

Abstract

This work presents the dynamic modeling of a vertical multi-effect evaporator plant designed and manufactured for its installation at a commercial concentrating solar power (CSP) plant, within the framework of EU H2020 project SOLWARIS (Solving Water Issues for CSP plants). The model has been developed using Modelica computational language and implemented in Dymola® software environment. The results from the validation show a good agreement against the design data, obtaining relative errors lower than 5%. The dynamic response of the plant against external disturbances of the motive steam mass flow rate, feedwater mass flow rate and condenser pressure has been investigated. The main results reveal that increasing the motive steam flow rate by 5% produces a similar increment of the water recovered (5.2%), although the concentrate salinity is raised to an unsafe operation zone (106%) that could lead to scaling issues in the evaporators. The same effect occurs when the feedwater is decreased by 5% from its nominal value, causing a significant rise in the concentrate salinity (163%). In those cases, the simultaneous and proportional variation of the motive steam and feedwater mass flow rates allows maintaining the outlet concentrate salinity far from scale formation limits.

Keywords: Dynamic model, Multi-effect Evaporation, Vertical Falling-film, Dymola, Sensitivity analysis

1. Introduction

Water consumption in concentrating solar power (CSP) plants is one of the major challenges this technology has to cope with since these plants are usually installed in arid or semi-arid locations with important water scarcity issues. The water reuse of wastewater streams from a CSP plant (i.e., the blowdown of the power block and cooling) seems a promising option to reduce the high water consumption required. This can be achieved by water treatment technologies that provide high-purity water, such as multi-effect evaporation (MEE), apt for mirror cleaning and for the make-up in the cooling tower and the power cycle. An added value of this option is that most CSP plants have a surplus of thermal energy (i.e., up to 30% of the total one demanded by the plant), which is dumped by the defocusing of some collectors, and it can be used for driving the thermal evaporation process. Therefore, the high external energy consumption required by this kind of water treatment plant would be saved.

In the frame of an EU H2020 project called SOLWARIS (Solving Water Issues for CSP plants) [1] a vertical falling-film MEE plant has been designed and manufactured at a relevant scale by the Spanish company INDETEC for water recovery purposes. The aim is its installation at a commercial CSP plant to produce a valuable product (almost pure water) that will be able to significantly reduce the wastewater discharge to the evaporation ponds and the raw water required by the CSP plant. To find the optimal operating conditions that lead to the maximum production of clean water and to the minimum electricity consumption (which is the greatest exergy destruction source apart from that corresponding to the thermal energy, assumed negligible in this case [2]), the mathematical modeling and computer simulation of the MEE plant is the first requisite.

Several MEE models have been developed and published in the scientific literature, but most of them are based on horizontal falling-film evaporators that use seawater as the working fluid. The first works found in the literature related to the modeling of vertical falling-film MEE plants are at steady-state and they are detailed hereinafter. Early in the 80s, Angeletti and Moresi [3] presented a model of an MEE unit used for the orange juice elaboration process. The model was validated successfully against data obtained from industrial MEE plants, using different correlations of the overall heat transfer coefficients (OHTCs). Khademi et al. [4] performed the modeling and optimization of a six-effect MEE used for desalination. In addition, a sensitivity analysis to study the effect of the variation of the feedwater temperature on the energy consumption and water produced was performed. It was found that an increase in the feedwater temperature resulted in a decrease in the external steam consumption and an increment of the water produced. Khanam & Mohanty [5] developed a simplified model of a seven-effect evaporator used for black liquor concentration. The model was validated against other published models and industrial data, obtaining a good prediction of the steam consumption (error < 3%). Srivastava et al. [6] presented the model of a falling film evaporator used for the sugar industry. The validation was done by the comparison with data from industrial plants, showing a maximum error of ±2% for the exit liquor concentration, vapor body temperature, and vapor bleed. However, the error of the OHTC was between -8.8% and +13%, with respect to the real values collected from the sugar industry. Finally, Sagharichiha et al. [7] developed a model of vertical tube falling film evaporators for desalination purposes. The model was validated by comparison with models published in the literature, and some significant deviations were found (relative error of about 20% in the mass flow rates).

However, the steady-state models are not generally useful for control and real-time optimization purposes, and these tasks are essential in MEE plants driven by solar energy that usually have to operate at partial load due to the variability of the solar irradiance. For control and optimization purposes, dynamic models are required in this framework. Some relevant works can be found in the literature in this respect. One of the first dynamic MEE models presented was done by Andre & Ritter [8] for a laboratory-scale double-effect evaporator. The model was based on mass and energy balances on the main elements of the system, and it fitted well with the experimental results. It was used to analyze the transient response against changes in the feed and steam mass flow rates. Quaak et al. [9] developed a dynamic model of a four-effect MEE plant based on first principles for control purposes. It was validated against measured data, showing good agreement. Winchester & Marsh [10] presented the model of a single-effect evaporator with mechanical vapor recompression for milk powder production. The model was used to develop control loops for the regulation of the effect temperatures, product dry mass fraction and product flowrate, but it was not validated. Stefanov and Hoo [10] presented a distributed-parameter model of a lamella-type evaporator used for black liquor concentration. The model was used to analyze the effect of the variation in the feed flow rate, feed dry solids content and wall temperature on the black liquor mass flow rate and dry solids content. The same authors later developed an extended model for an MEE plant [12]. This extended model was validated against steady-state data taken from an industrial plant, resulting in good agreement with model predictions. Kumar et al. [13] developed an MEE plant mathematical model for the paper industry. The model was based on mass and energy balances and was able to simulate different flow arrangements. The dynamic effect of disturbances on the feed flow rate, temperature and concentration, together with the heating steam temperature, were analyzed. No validation of the model was shown, though. Finally, Bojnourd et al. [14] presented a dynamic model for a four-effect industrial MEE plant for milk powder production, using both a lumped-parameter and a distributed-parameter approximation. The models were validated against data obtained from the industrial plant showing good agreement with predicted values. It was found that the lumped model has similar reliability in comparison with the distributed model, with a simpler structure and requiring less calculation time.

This paper presents a detailed dynamic model of a three-effect MEE unit to be integrated at a commercial CSP plant for water reuse. The model is based on the one presented by Bojnourd et al. [14] for the evaporators, but it includes relevant contributions in the entire plant modeling, modifications in the structure of the equations and considers relevant additions such as the flashing process, recirculation of the concentrate in each effect, thermal losses and the pumping power consumption. This model thus allows a better precision for control and optimization purposes. The paper shows the validation of the model against steady-state conditions (i.e., the corresponding to the nominal conditions of the plant) and the assessment of the plant efficiency (in terms of electricity and energy consumption) and the total water recovered with the variation of several operational variables, which allows identifying the most favorable operating conditions. Finally, the dynamic response of the system against disturbances in the main operating variables is presented.

2. Process description

The MEE plant (see Fig. 1) is composed of three long-tube vertical falling film evaporators (namely H_1, H_2 and H_3), three liquid-vapor separators (C_1, C_2 and C_3) and a surface condenser (SC). The plant also has two plate heat exchangers (PHX_1 and PHX_2), a thermocompressor (TVC), a separation bottle (SB), and eight pumps (P01-P08).

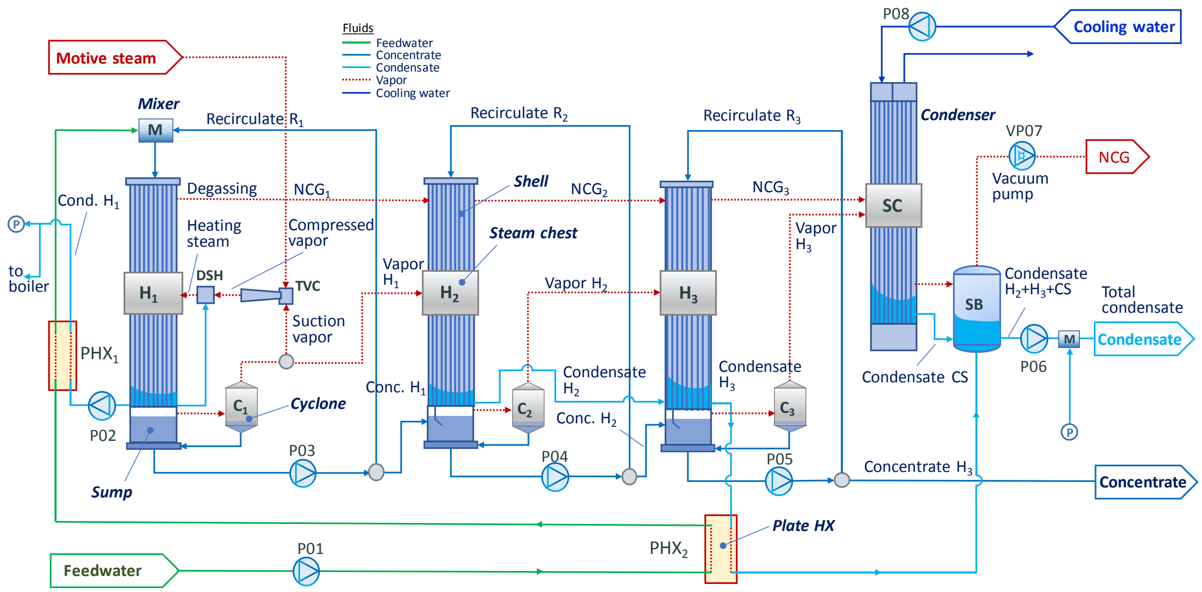

Fig. 1. Scheme of the MEE plant.

The working principle of the MEE plant is essentially the evaporation of the feedwater using external vapor, producing steam and concentrated water. This process is done in several stages (called effects) to take advantage of the heat produced in the evaporation process within one effect, making the process more efficient. A profile of decreasing pressures and temperatures is created along the effects while the condenser pressure is imposed by a vacuum pump (VP07).

The feedwater enters the plate heat exchanger PHX_2, where is warmed up when heat is exchanged with the condensate produced in effect H_3. Then, it enters the plate heat exchanger PHX_1, where is further heated up with sensible heat of the condensate produced in H_1. Before entering the tubes of the evaporator H_1, the feedwater is mixed with a recirculating flow of the concentrate solution generated in the effect. This recirculation flow takes place in each effect and aims to avoid the formation of dry spots in the tubes. The feed is distributed at the top of the tubes, flowing inside them downwards and forming a thin falling film around the tubes. This film partially evaporates along the tubes, so that at the bottom of them, vapor and concentrate flow can be found. The mixture reaches the lowest part of the tubes, called the sump, which is physically separated from the shell of the effect. The sump is a vessel at the bottom of the effect where part of the concentrate stream is accumulated up to a certain level. The mixture is then separated in the cyclonic box C_1. Part of the vapor produced in H_1 is recompressed in the thermocompressor using motive steam produced at medium/high pressure in a steam generator, and the resulting compressed vapor is directed to the steam chest of H_1, where condenses and releases its phase change heat to the falling film circulating inside the tubes. The vapor produced in H_1 is used as heating steam in H_2, while the concentrated flow is used as the feed stream to H_2, repeating the condensation-evaporation process. Note that, apart from the vapor generated by boiling, an additional amount of vapor is produced by flashing when the concentrate solution from H_1 enters H_2, and the one from H_2 enters H_3. There is also flash evaporation when the condensate from H_2 enters the shell of H_3. Finally, the vapor produced in H_3 is condensed in the surface condenser SC and, together with the condensates coming from H_2 and H_3, all of them are mixed in the separation bottle. The final concentrate flow comes from the cyclonic box C_3. Part of the condensate produced in H_1 is collected together with the condensates in H_2, H_3 and SC, while the rest (equal to the motive steam flow) comes back to the condensate tank of the steam generator. Note also that part of the condensate produced in H_1 is used in a desuperheater (DSH) to achieve saturating conditions in the compressed vapor at the outlet of the thermocompressor. In addition, a small fraction of the vapor produced in each effect is dragged together with the non-condensable gases (NCG) by the vacuum system.

The main features of the MEE plant at nominal conditions are depicted in Table 1.

Table 1. Main characteristics of the MEE plant at nominal conditions.

Concept	Value
Type	3-effect with TVC
Recovery ratio	91%
Evaporation flow rate (kg/h)	7502
Feed flow rate (kg/h) (@20°C)	8250
Concentrate flow rate (kg/h)	750
Steam consumption (kg/h) (@10.5 bar with TVC)	2002
Cooling flow rate (m^3/h) (@33°C DT=6°C)	175

3. Modeling

The developed MEE dynamic model is based on that presented by Medhat Bojnourd et al. [14] with required additions and modifications (recirculation of the concentrate solution, flashing of brine and distillate, fouling in the heat exchangers and thermal losses in the effects).

The model consists of mass and energy balance equations applied to each component of the plant, together with the heat transfer equations associated with the heat exchangers. The mass balances of the falling film flow rate for the external condensation and internal evaporation in the effects, together with the salts content of the falling film, have been modeled using dynamic equations. The rest of the components have been modeled in stationarity conditions, assuming they have small inertia compared to the evaporation/condensation process within the evaporators. The cyclonic boxes have not been modeled because they do not imply any significant change in the operating variables (mass flow rate, temperature, pressure, etc.). The main assumptions considered are described as follows:

- Lumped-parameter models have been chosen for the components of the system.
- The evaporated water is considered salt-free.
- The effect of the NCG on heat transfer has been neglected.
- The energy accumulation on the falling film and in the tube has not been considered (stationary energy balances).
- Average values of some variables (mass flow rate of the falling film outside and inside the tubes, the residence time of the falling film, the velocity of the falling film, etc.) have been taken into account in the evaporator tubes, with the average-making parameter α set as 0.5.
- Fouling factors have been assumed in H_1 (tube side $0.4\cdot10^{-4}$ °C·m^2/W), H_2 ($0.7\cdot10^{-4}$ °C·m^2/W) and H_3 ($8.3\cdot10^{-4}$ °C·m^2/W) evaporators and end condenser ($13\cdot10^{-4}$ °C·m^2/W) due to the possibility of scale events (personal communication from the manufacturer).
- The residence time and the velocity of the falling film (0.75 m/s) have been assumed constant (personal communication from the manufacturer).
- Thermal losses in the effects have been assumed to be 2% of the total heat rate of evaporation, in accordance with data provided by the plant manufacturer.

The model has been implemented in Dymola® [15], which is a commercial modeling environment based on Modelica, an object-oriented modeling language for complex systems. Modelica is declarative, allows acausal modeling, the use of hierarchical structures, multi-domain simulation and visual component programming.

In the next section, the evaporator model is described, which is identical for all three effects. Then, the model for each effect and the rest of the components is defined.

3.1 Evaporator model

The evaporator model has been divided into three components: the outside tubes, where the heating steam coming from the thermocompressor (for effect H_1) and from the previous effect (in the case of H_2 and H_3) condenses; the tube wall, where the condensation heat is transferred to the inside tubes; and the inside tubes, where part of the feedwater plus the recirculate flow (in the case of the effect H_1) or only the recirculate flow (in the case of effects H_2 and H_3) evaporates.

3.1.1 Outside tubes

The control volume (CV) is delimited by the falling film downwards the outer surface of a generic evaporator tube, as shown in Fig. 2. Note that the thickness of the falling film is assumed to be zero at the top of the tube and, due to gravity and accumulation of liquid on the external surface of the tube, the thickness grows downwards being the maximum at the bottom. The energy balance in the CV is established as follows:

$$\frac{dE_{cd}}{dt} = 0 = -\dot{Q}_{cd} + \lambda\dot{m}_{cd} \Rightarrow \dot{Q}_{cd} = \lambda\dot{m}_{cd} \tag{1}$$

where E_{cd} (J) is the internal energy, $\dot{Q}_{cd}$ (W) is the condensation heat rate, λ (J/kg) is the specific enthalpy of condensation, and $\dot{m}_{cd}$ (kg/s) is the mass flow rate of condensate.

The mass balance in the CV is established by Eq. (2):

$$\frac{dM_{cd}}{dt} = \dot{m}_{cd,i} - \dot{m}_{cd,o} + \dot{m}_{cd} \tag{2}$$

where M_{cd} (kg) is the mass of the falling film of condensate outside the tube, $\dot{m}_{cd,i}$ (kg/s) is the inlet mass flow rate of condensate at the top of the tube and $\dot{m}_{cd,o}$ (kg/s) is the outlet mass flow rate of condensate at the bottom of the tube. The vapor around the tube, at T_s (K), condenses when it reaches the tube wall, which is at a lower temperature, T_{wo} (K).

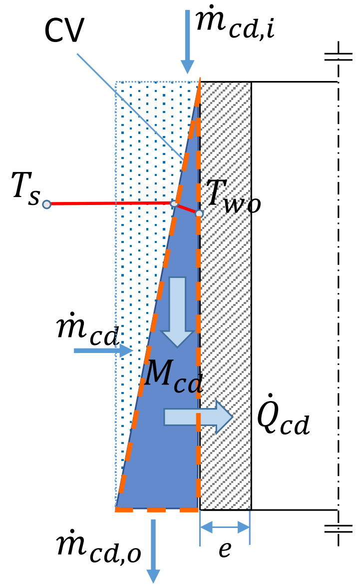

Fig. 2. Scheme of the CV for the outside condensation.

The mass flow rate of condensate outside the tube is determined with Eq. (3):

$$M_{cd} = \tau_{cd,av}\dot{m}_{cd,av} \tag{3}$$

where $\dot{m}_{cd,av}$ (kg/s) is the average mass flow rate of condensate outside the tube, and $\tau_{cd,av}$ (s) is the average residence time of the falling film, calculated with Eq. (4):

$$\tau_{cd,av} = \frac{L}{v_{cd,av}} \tag{4}$$

where L (m) is the length of the tube and $v_{cd,av}$ (m/s) is the average velocity of the condensate outside the tube.

The average values of a generic variable N_{av} (representing any other average variable, such as velocity, mass flow rate, etc.) can be obtained with Eq. (5):

$$N_{av} = \alpha N_i + (1-\alpha)N_o \tag{5}$$

where α is the average-making parameter, and N_i and N_o are the inlet and outlet values of the variable N. The value of α is in the range 0 – 1.

Substituting Eqs. (3) and (4) and the average values in Eq. (2), the following equation is obtained:

$$\frac{d\dot{m}_{cd,o}}{dt} = \frac{v_{cd,av}}{L(1-\alpha)}(\dot{m}_{cd,i} - \dot{m}_{cd,o} + \dot{m}_{cd}) - \frac{\alpha}{(1-\alpha)}\frac{d\dot{m}_{cd,i}}{dt} \tag{6}$$

3.1.2 Tube wall

The heat transfer equation in the tube wall establishes that the heat rate transferred by conduction, $\dot{Q}_{tr}$ (W), is a function of the thermal resistance of the tube, R_w (K/W), and the temperature difference between the outside tube wall, T_{wo} (K), and inside tube wall, T_{wi} (K):

$$\dot{Q}_{tr} = \frac{1}{R_w}(T_{wo} - T_{wi}) \tag{7}$$

The thermal resistance of the tube is defined by:

$$R_w = \frac{ln\left(\frac{D_o}{D_i}\right)}{2\pi L \cdot k_w} \tag{8}$$

with D_o (m) and D_i (m) being the external and internal diameters of the tube, respectively, and k_w (W/(m·K)) is the thermal conductivity of the tube.

3.1.3 Inside tubes

The model of the feedwater evaporation inside the tubes of the evaporator is similar to that one of the external condensation. The corresponding CV is shown in Fig. 3. In this case, it has been assumed a falling film profile with decreasing thickness due to the evaporation. Note that for the evaporator H_1 the energy balance is slightly different because the feedwater is subcooled and needs to be warmed up to saturation conditions. Therefore, an additional term representing the sensible heat is added to the energy balance as follows:

$$\frac{dE_{ev}}{dt} = 0 = \dot{Q}_{ev} - \lambda\dot{m}_{ev} - \dot{m}_i\bar{c}_p(T - T_i) \Rightarrow \dot{Q}_{ev} = \lambda\dot{m}_{ev} + \dot{m}_i\bar{c}_{p,i}(T - T_i) \tag{9}$$

where $\dot{Q}_{ev}$ (W) is the evaporation heat rate, $\dot{m}_{ev}$ (kg/s) is the mass flow rate of falling film evaporated, $\dot{m}_i$ (kg/s) is the inlet mass flow rate of the liquid film (feedwater plus the recirculating flow) at the top of the tube, $\bar{c}_{p,i}$ (J/(kg·K)) is the average specific heat at constant pressure between T and T_i, T (K) is the temperature of the falling film inside the tube (equal to the outlet falling film temperature), and T_i (K) is the falling film inlet temperature (subcooled) at the top of the tube, coming from the mixer.

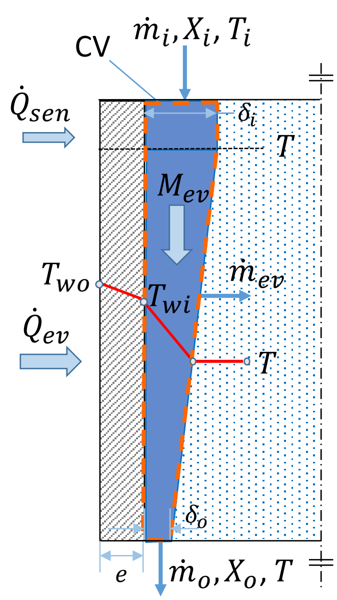

Fig. 3. Scheme of the CV for the inside falling film evaporation.

For evaporators H_2 and H_3 there is no preheating section, and the energy balance is as follows:

$$\frac{dE_{ev}}{dt} = 0 = \dot{Q}_{ev} - \lambda \dot{m}_{ev} \Rightarrow \dot{Q}_{ev} = \lambda \dot{m}_{ev} \tag{10}$$

The vapor at the outlet of the tubes is considered to be in thermal equilibrium with the liquid, whose temperature (T) is equal to the saturation temperature at the outlet of the tubes (T_{sat}) plus the boiling point elevation (BPE) of the solution due to the salt content:

$$T = T_{sat} + BPE \tag{11}$$

The mass balance equation applied to the same CV is as follows:

$$\frac{dM_{ev}}{dt} = \dot{m}_i - \dot{m}_o - \dot{m}_{ev} \tag{12}$$

where M_{ev} (kg) is the mass of falling film inside the tube, $\dot{m}_o$ (kg/s) is the outlet mass flow rate of liquid film at the bottom of the tube. Defining the falling film residence time and the average values of the liquid film velocity and mass flow rate, Eqs. (13) and (14), respectively, the mass balance is rearranged and expressed by Eq. (15):

$$\tau_{ev,av} = \frac{L}{v_{ev,av}} \tag{13}$$

$$M_{ev} = \tau_{ev,av} \dot{m}_{av} \tag{14}$$

$$\frac{d\dot{m}_o}{dt} = \frac{v_{ev,av}}{L(1-\alpha)} (\dot{m}_i - \dot{m}_o - \dot{m}_{ev}) - \frac{\alpha}{(1-\alpha)} \frac{d\dot{m}_i}{dt} \tag{15}$$

where $\dot{m}_{av}$ (kg/s) is the average mass flow rate of the falling film.

The falling film thickness at the top (δ_i) and at the bottom (δ_o) of the tubes can be determined considering the evaporator geometry that is known:

$$\delta_i = \left(D_i - \sqrt{D_i^2 - 4 \cdot A_{ci}/\pi} \right) / 2 \tag{16}$$

$$\delta_o = \left(D_i - \sqrt{D_i^2 - 4 \cdot A_{co}/\pi} \right) / 2 \tag{17}$$

where A_{ci} and A_{co} (m^2) are the areas of the falling film crown at the top and the bottom of the tube, respectively, and they can be calculated as follows:

$$A_{ci} = \frac{\dot{V}_i}{v_i} = \frac{\dot{m}_i/\rho_i}{v_i} \tag{18}$$

$$A_{co} = \frac{\dot{V}_o}{v_o} = \frac{\dot{m}_o/\rho_o}{v_o} \tag{19}$$

where $\dot{V}_i$ and $\dot{V}_o$ (m^3/s), v_i and v_o (m/s), and ρ_i and ρ_o (kg/m^3) are the volumetric flow rate, velocity and density of the liquid at the top and the bottom of the tube, respectively.

3.1.4 Heat transfer equations

The heat transfer equations for the evaporator establish that the heat released by the condensation of the external vapor outside the tubes is transferred to the internal falling film for its partial evaporation. The total heat transfer rate in the tubes, $\dot{Q}_{tot}$, is determined by Eqs. (20)-(23):

$$\dot{Q}_{tot} = U_i\, A_i\, (T_s - T)N_t \tag{20}$$

$$\dot{Q}_{tot} = \dot{Q}_{sen,tot} + \dot{Q}_{ev,tot} \tag{21}$$

$$\dot{Q}_{sen,tot} = \dot{m}_i \bar{c}_p (T - T_i) N_t \tag{22}$$

$$\dot{Q}_{ev,tot} = \dot{m}_{ev} \lambda N_t \tag{23}$$

where U_i (W/(m^2·K)) is the overall heat transfer coefficient referred to the internal area, A_i (m^2) is the inner surface area of one tube, N_t is the number of tubes, $\dot{Q}_{sen,tot}$ (W) is the total sensible heat rate, and $\dot{Q}_{ev,tot}$ (W) is the total heat rate of evaporation. Note that the sensible term in the equation is used only for H_1 evaporator. The equation to determine U_i is a function of the internal heat transfer surface, as follows:

$$U_i = \frac{1}{\sum R_i} = \frac{1}{R_{cv,int} + R_{fi} + R_w + R_{fo} + R_{cv,ext}}$$
$$= \frac{1}{\frac{1}{h_i} + R_{fi} + \frac{D_i ln(D_o/D_i)}{2k_w} + \frac{D_i}{D_o} \cdot R_{fo} + \frac{D_i}{D_o} \cdot \frac{1}{h_o}} \tag{24}$$

where h_i and h_o (W/(m^2·K)) are the internal and external convective heat transfer coefficients, respectively, R_i ((m^2·K)/W) is the thermal resistance of element i, $R_{cv,int}$ and $R_{cv,ext}$ are the internal and external convective thermal resistances, respectively, and R_{fi}, R_{fo} ((m^2·K)/W) are the internal and external fouling factors, respectively.

Several correlations of the convective heat transfer coefficient have been analyzed to select those that better fit the nominal conditions of the plant. From the analysis, the best fitting was found for the correlation presented by Shmerler & Muddawar [16] in the case of the internal evaporation and the correlation of Labuntsov [17] for the external condensation. More information can be found in Appendix A.

3.2 Effect H_1

This section presents the mass and energy balances for effect H_1 and the modeling equations of the associated components: the mixer (M), the thermocompressor and the desuperheater.

3.2.1 Mass and energy balances

The CV established for effect H_1 includes the evaporator, TVC, mixer, cyclonic box and recirculation stream (see Fig. 4). Note that the recirculation flow has the same thermodynamic properties that the outlet concentrate stream.

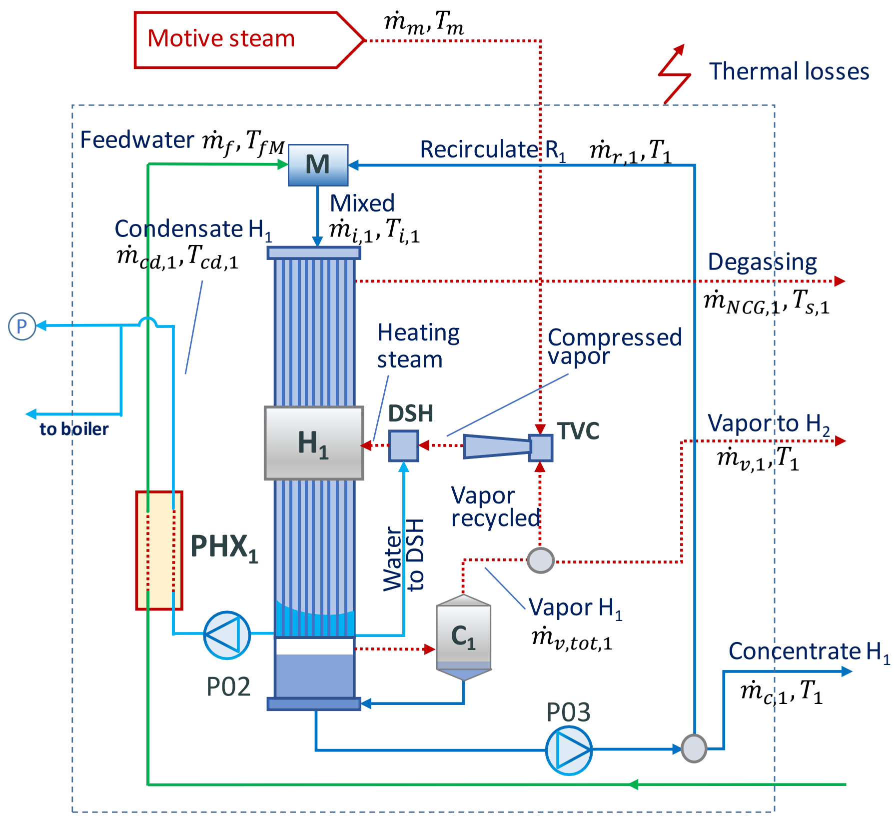

Fig. 4. Control volume for the global mass and energy balances applied in effect H_1. Note that part of the total condensate in H_1 returns to the boiler while the rest is mixed with the other condensates in point P.

The mass and energy balances for this CV are as follows:

$$\frac{dM_{L,1}}{dt} = \rho_{L,1}\pi R_{H1}^2 \frac{dL_{H1}}{dt} = \dot{m}_f - (\dot{m}_{c,1} + \dot{m}_{v,tot,1}) \tag{25}$$

$$\frac{dM_{L,1}}{dt} = \rho_{L,1}\pi R_{H1}^2 \frac{dL_{H1}}{dt} = (\dot{m}_f + \dot{m}_m) - (\dot{m}_{NCG,1} + \dot{m}_{cd,1} + \dot{m}_{v,1} + \dot{m}_{c,1})$$

$$\dot{m}_f h_f + \dot{m}_m h_m = \dot{m}_{NCG,1} h_{NCG,1} + \dot{m}_{v,1} h_{v,1} + \dot{m}_{cd,1} h_{cd,1} + \dot{m}_{c,1} h_{c,1} + \dot{Q}_{loss,1} \tag{26}$$

where $M_{L,1}$ (kg) is the mass of liquid in the sump of H_1 , $\rho_{L,1}$ (kg/m^3) is the density of the liquid in the sump of H_1, R_{H1} (m) is the radius of the sump of H_1, L_{H1} (m) is the level of the liquid in the sump of H_1, $\dot{m}_f$, $\dot{m}_m$, $\dot{m}_{NCG,1}$, $\dot{m}_{v,1}$, $\dot{m}_{v,tot,1}$, $\dot{m}_{cd,1}$, $\dot{m}_{c,1}$ (kg/s), and h_f, h_m, $h_{NCG,1}$, $h_{v,1}$, $h_{cd,1}$,

$h_{c,1}$ (J/kg) are the mass flow rates and specific enthalpy of feedwater, motive steam, vapor entrained by the extraction of the NCG, vapor going to H_2, condensate and concentrate streams in H_1, respectively, while $\dot{Q}_{loss1}$ (W) is the heat rate loss in effect H_1.

The salt balance is established in this CV through Eq. (27):

$$\frac{d\left(M_{L,1}X_{av,1}\right)}{dt} = \dot{m}_f X_f - \dot{m}_{c,1}X_{c,1} \tag{27}$$

where, $X_{av,1}$ (ppm) is the average salt content in H_1, and X_f, $X_{c,1}$ (ppm) are the salt content of the feed inlet and concentrate outlet flows, respectively. Substituting the definitions of $M_{L,1}$ and $X_{av,1}$, the Eq. (27) is rearranged as follows:

$$\frac{dX_{o,1}}{dt} = \frac{\left[\dot{m}_f\left(X_f - X_{av,1}\right) - \dot{m}_{c,1}\left(X_{o,1} - X_{av,1}\right) + \dot{m}_{v,tot,1}X_{av,1}\right]}{M_{L,1}(1-\alpha)} - \frac{\alpha}{(1-\alpha)}\frac{dX_f}{dt} \tag{28}$$

3.2.2 Mixer

The subcooled feedwater, before entering the evaporator tubes in effect H_1, is blended with the recirculated concentrate solution in a mixer, which is at saturation conditions. Applying the mass and energy balances on the mixer, the feedwater mass flow rate and temperature at the outlet of the mixer can be determined as follows:

$$\dot{m}_f + \dot{m}_{r,1} = \dot{m}_{i,1} \tag{29}$$

$$\dot{m}_f h_{fM} + \dot{m}_{r,1}h_{r,1} = \dot{m}_{i,1}h_{i,1} \tag{30}$$

where $\dot{m}_{r,1}$ (kg/s) is the mass flow rate of the recirculated concentrate solution in H_1, $\dot{m}_{i,1}$ (kg/s) is the mass flow rate of the feedwater at the outlet of the mixer, and h_{fM}, $h_{r,1}$, and $h_{i,1}$ (J/kg) are the specific enthalpies of the feedwater at the inlet of the mixer, recirculate and outlet of the mixer, respectively.

3.2.3 *Thermocompressor*

The thermocompressor uses high/medium pressure motive steam obtained from a steam generator to recompress low-pressure steam extracted from the first effect (see Fig. 5). A stationary model has been considered since its dynamics is much faster than that of the evaporator [18].

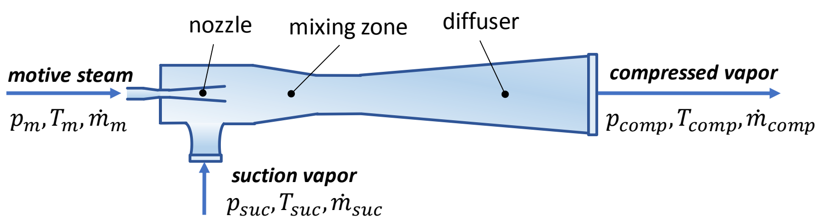

Fig. 5. Scheme of the thermocompressor.

The mass and energy balance equations are defined by Eqs. (31)-(32):

$$\dot{m}_m + \dot{m}_{suc} = \dot{m}_{comp} \tag{31}$$

$$\dot{m}_m h_m + \dot{m}_{suc} h_{suc} = \dot{m}_{comp} h_{comp} \tag{32}$$

where $\dot{m}_{suc}$ and $\dot{m}_{comp}$ (kg/s) are the suction and compressed vapor mass flow rates, respectively, and h_{suc}, and h_{comp} (J/kg) are the specific enthalpies of the suction and compressed vapor flows, respectively.

Two empirical models from the scientific literature [19,20] have been analyzed and compared versus the design data. The comparison has been made in terms of the entrainment ratio Ra (Eq. (33), defined as the ratio of motive steam mass flow rate to suction/entrainment vapor mass flow rate), resulting that the correlation with the best fitting was the one from El-Dessouky [19], which has been selected for its implementation in the model. Eqs. (33)-(35) present the empirical correlations used by El-Dessouky for the calculation of the entrainment ratio:

$$Ra = 0.296 \cdot \left(\frac{p_{comp}^{1.19}}{p_{suc}^{1.04}}\right) \cdot \left(\frac{p_m}{p_{suc}}\right)^{0.015} \cdot (PCF/TCF) \tag{33}$$

$$PCF = 3 \cdot 10^{-7} \cdot p_m^2 - 0.0009 \cdot p_m + 1.6101 \tag{34}$$

$$TCF = 2 \cdot 10^{-8} \cdot T_{suc}^2 - 0.0006 \cdot T_{suc} + 1.0047 \tag{35}$$

where p_{comp}, p_{suc}, and p_m (kPa) are the pressures of the compressed vapor, suction vapor, and motive steam, respectively, PCF is the motive steam pressure correction factor, TCF is the suction vapor temperature correction factor, and T_{suc} (°C) is the suction vapor temperature.

3.2.4 Desuperheater

As mentioned in the process description, the desuperheater is in charge to temper the compressed vapor temperature from superheating to saturation conditions by using a condensate stream that is extracted from the condensate section of H_1 (see Fig. 6). The mass and energy balances applied to this component are presented in Eqs. (36) - (37):

$$\dot{m}_{comp} + \dot{m}_{dsh} = \dot{m}_{sat} \tag{36}$$

$$\dot{m}_{comp}h_{comp} + \dot{m}_{dsh}h_{dsh} = \dot{m}_{sat}h_{sat} \tag{37}$$

where $\dot{m}_{comp}$, $\dot{m}_{dsh}$, $\dot{m}_{sat}$ (kg/s) and h_{comp}, h_{dsh}, h_{sat} (kJ/kg) are the mass flow rates and specific enthalpies of the compressed vapor, condensate, and saturated steam, respectively.

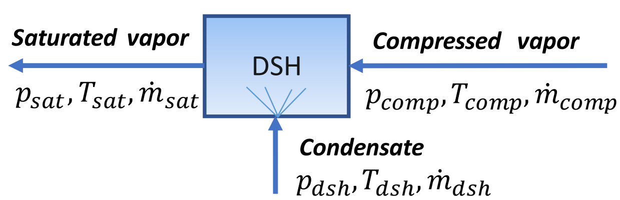

Fig. 6. Process scheme of the desuperheater.

3.3 Effects H_2 and H_3

The set of equations of effects $H_2$and H_3 models have a similar structure, except for the flashing of the condensate coming from H_2 when entering the shell of H_3. The models of these effects consider the flashing process of the concentrate solution coming from the previous effect, which enters the sump and is mixed with the concentrate produced in the evaporator. Also, as for H_1, global mass and energy balances are applied to a CV delimited by the whole effect.

3.3.1 Mass and energy balances

The CV defined for effects H_i (i = 2, 3) is delimited by the effect itself and the recirculation flow, as can be seen in Fig. 7. The mass and energy balances in this CV are as follows:

$$\frac{dM_{L,i}}{dt} = \rho_{L,i}\pi R_{Hi}^2 \frac{dL_{Hi}}{dt} = \dot{m}_{c,i-1} - (\dot{m}_{c,i} + \dot{m}_{v,i}) \tag{38}$$

$$\begin{aligned} &\dot{m}_{c,i-1}h_{c,i-1} + \dot{m}_{v,i-1}h_{v,i-1} + \dot{m}_{NCG,i-1}h_{v,i-1} \left\{+\, \dot{m}_{cd,i-1}h_{cd,i-1}\right\} \\ &\qquad = \dot{m}_{NCG,i}h_{NCG,i} + \dot{m}_{v,i}h_{v,i} + \dot{m}_{cd,i}h_{cd,i} + \dot{m}_{c,i}h_{c,i} + \dot{Q}_{loss,i} \end{aligned} \tag{39}$$

where $M_{L,i}$ (kg) is the mass of liquid in the sump of H_i, $\rho_{L,i}$ (kg/m^3) is the density of the liquid in the sump of H_i, R_{Hi} (m) is the radius of the sump of H_i, L_{Hi} (m) is the level of the liquid in the sump of H_i, $\dot{m}_{c,i}$, $\dot{m}_{v,i}$, $\dot{m}_{NCG,i}$, $\dot{m}_{cd,i}$ (kg/s), and $h_{c,i}$, $h_{v,i}$, $h_{NCG,i}$, $h_{cd,i}$ (J/kg) are the mass flow rates and specific enthalpies of the concentrate, the vapor produced, the vapor entrained by the extraction of the NCG, and the condensate streams of H_i, respectively, and $\dot{Q}_{loss,i}$ (W) is the heat rate loss in effect H_i. Note that in Eq. (39) for effect H_2 the term $\dot{m}_{cd,i-1}h_{cd,i-1}$ does not exists because there is no condensate stream going from H_1 to H_2.

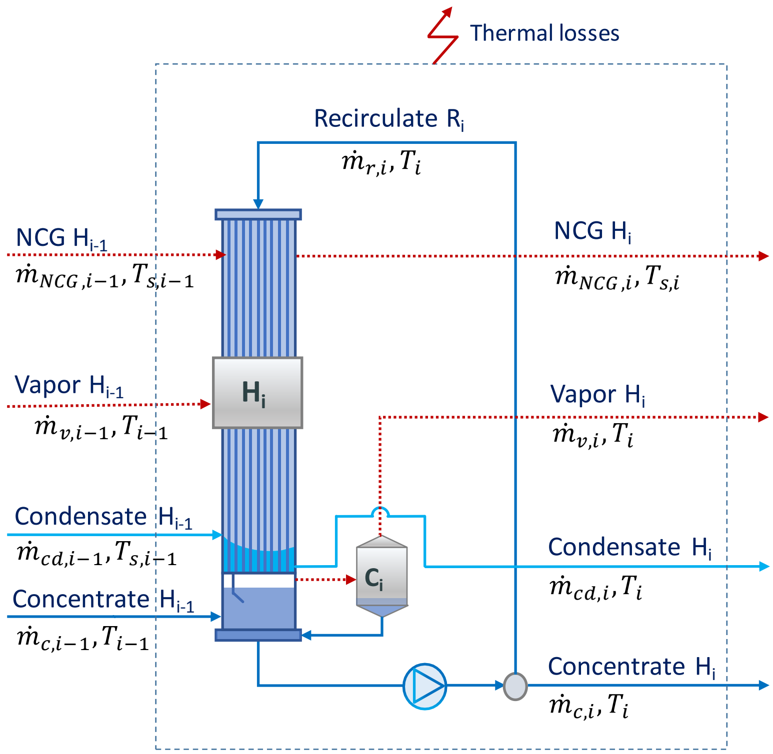

Fig. 7. CV for the global mass, salt and energy balances applied in effect H_i (i= 2,3).

The salt balance is described by Eq. (40):

$$\frac{d(M_{L,i}X_{av,i})}{dt} = \dot{m}_{c,i-1}X_{o,i-1} - \dot{m}_{c,i}X_{o,i} \tag{40}$$

where, $X_{av,i}$ (ppm) is the average salt content in H_i, and $X_{o,i}$ (ppm) is the salt content of the concentrate outlet flow in H_i.

Then, Eq. (40) is rewritten as follows:

$$\frac{dX_{o,i}}{dt} = \frac{[\dot{m}_{c,i-1}(X_{o,i-1} - X_{av,i}) - \dot{m}_{c,i}(X_{o,i} - X_{av,i}) + \dot{m}_{v,i}X_{av,i}]}{M_{L,H2}(1-\alpha)} - \frac{\alpha}{(1-\alpha)}\frac{dX_{o,i-1}}{dt} \tag{41}$$

3.3.2 Concentrate flash in H_2 and H_3

The concentrate from H_{i-1} , at saturated conditions, enters the sump of H_i, that is at lower pressure, taking place flash evaporation that generate an additional amount of vapor, which is added to the vapor produced inside the tubes of H_i (see Fig. 8). Note that the concentrate flashes inside the sump of the evaporator, however, for the sake of clarity, a flashing box has been added to establish the governing equations of the flashing process.

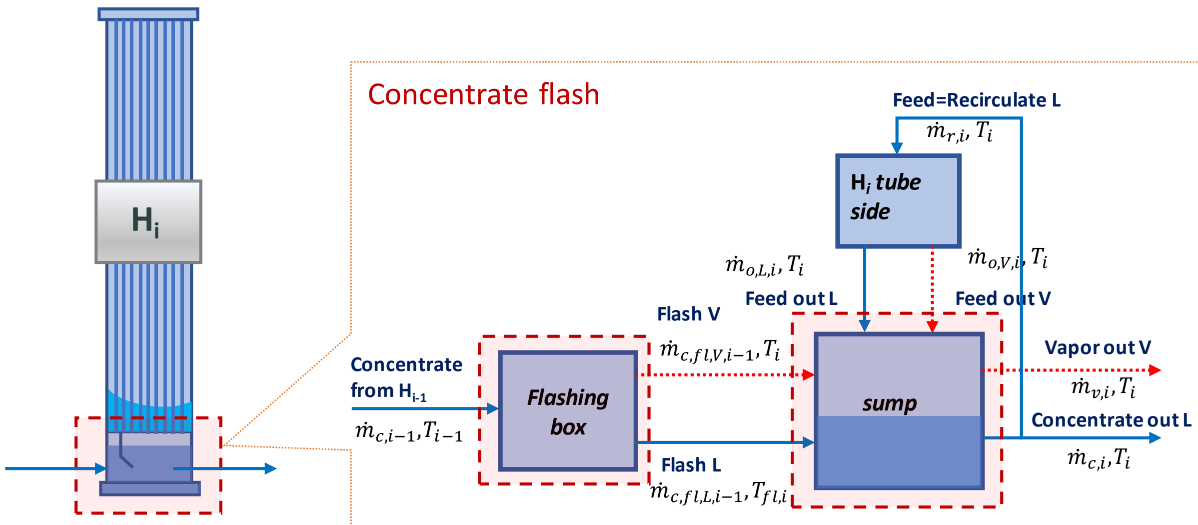

Fig. 8. Scheme of the concentrate flash process in evaporators H_2 and H_3.

The energy balance applied to the flashing box is as follows:

$$\dot{m}_{c,fl,V,i-1}\lambda_{fl} = \dot{m}_{c,i-1}\bar{c}_{p,fl}\left(T_{i-1} - T_{fl,i}\right) \tag{42}$$

where $\dot{m}_{c,fl,V,i-1}$ (kg/s) is the mass flow rate of flash vapor produced from the concentrate solution coming from H_{i-1}, λ_{fl} (J/(kg-K)) is the specific enthalpy of vaporization, $\dot{m}_{c,i-1}$ (kg/s) is the mass flow rate of concentrate solution coming from H_{i-1}, $\bar{c}_{p,fl}$ (J/(kg·K)) is the average specific heat at constant pressure, T_{i-1} (K) is the temperature of the concentrate coming from H_{i-1} and $T_{fl,i}$ (K) is the temperature of the remaining concentrate after the flashing process. The flashed concentrate reduces its temperature to a value that is above the equilibrium temperature in H_i by an amount named non-equilibrium allowance (NEA).

$$T_{fl,i} = T_i + NEA_i \tag{43}$$

The NEA can be determined with the following correlation presented by Miyatake et al. [21]:

$$NEA_i = 33\frac{(T_{i-1} - T_i)^{0.55}}{T_i} \tag{44}$$

The mass balances in the sump, both for the liquid and the vapor phases, are as follows:

$$\dot{m}_{c,fl,L,i-1} + \dot{m}_{o,L,i} = \dot{m}_{c,i} + \dot{m}_{r,i} \tag{45}$$

$$\dot{m}_{c,fl,V,i-1} + \dot{m}_{o,V,i} = \dot{m}_{v,i} \tag{46}$$

where $\dot{m}_{c,fl,L,i-1}$, $\dot{m}_{o,L,i}$, $\dot{m}_{c,i}$, $\dot{m}_{r,i}$ (kg/s) are the mass flow rates of the concentrate after the flashing process, the concentrate at the outlet of the tubes of H_i, the concentrate at the outlet of the effect, and the recirculate, respectively, while $\dot{m}_{c,fl,V,i-1}$, $\dot{m}_{o,V,i}$, $\dot{m}_{v,i}$ (kg/s) are the mass flow rates of the vapor produced by flash, the vapor produced inside the tubes of H_i, and the total vapor exiting the effect, respectively.

3.3.3 Condensate flash in H_3

In addition to the flash of the concentrate in effect H_3, there is also flashing of the distillate coming from H_2. The condensate produced in H_2 enters the shell of H_3 to take advantage of the residual heat content of this stream. As it is saturated, when it is discharged to a lower pressure space, part of it flashes, generating additional vapor (see Fig. 9).

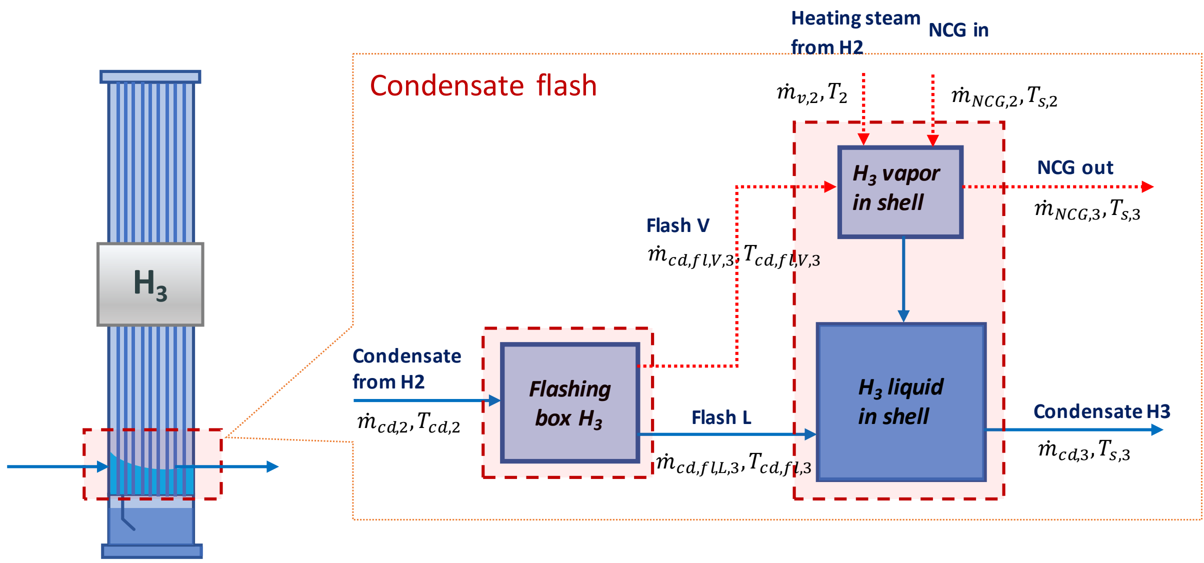

Fig. 9. Scheme of the condensate flash process in the evaporator H_3.

In the case of the flash evaporation caused by the condensate, the amount of vapor produced can be determined through Eqs. (47)-(49):

$$\dot{m}_{cd,fl,V,2}\lambda_{cd,fl} = \dot{m}_{cd,2}\bar{c}_{p,cd,fl}\left(T_{cd,2} - T_{cd,fl,3}\right) \tag{47}$$

$$T_{cd,fl,3} = T_3 + NEA_{cd,3} \tag{48}$$

$$NEA_{cd,3} = 33\frac{\left(T_{cd,2} - T_{cd,fl,3}\right)^{0.55}}{T_{cd,fl,V,3}} \tag{49}$$

where $\dot{m}_{cd,fl,V,2}$ (kg/s) is the mass flow rate of flash vapor produced from the condensate coming from H_2, $\lambda_{cd,fl}$ (J/(kg·K)) is the specific enthalpy of condensation of the vapor, $\dot{m}_{cd,2}$ (kg/s) is the mass flow rate of condensate coming from H_2, $\bar{c}_{p,cd,fl}$ (J/(kg·K)) is the average specific heat at constant pressure of the condensate, $T_{cd,2}$ (K) is the temperature of the condensate coming from H_2, $T_{cd,fl,V,3}$ (K) is the temperature of the vapor produced (which is assumed to be equal to the vapor temperature in the shell of H_3, $T_{s,3}$) and $T_{cd,fl,3}$ (K) is the temperature of the remaining condensate after flashing.

The mass balance equation in the shell of H_3 is as follows:

$$\dot{m}_{cd,fl,V,2} + \dot{m}_{cd,fl,L,2} + \dot{m}_{NCG,2} + \dot{m}_{v,2} = \dot{m}_{NCG,3} + \dot{m}_{cd,3} \tag{50}$$

where $\dot{m}_{cd,fl,V,2}$, $\dot{m}_{cd,fl,L,2}$, $\dot{m}_{NCG,2}$, $\dot{m}_{v,2}$, $\dot{m}_{NCG,3}$ and $\dot{m}_{cd,3}$ (kg/s) are the mass flow rates of flash vapor produced from the condensate coming from H_2, the condensate that remains without flashing, the vapor dragged with the NCG coming from H_2, the heating steam coming from H_2, the vapor dragged with the NCG leaving H_3, and the total condensate produced in H_3, respectively.

3.4 Final condenser

The final condenser SC (see Fig. 10) is in charge of condensing the vapor coming from the last effect and the steam dragged with the NCG by the vacuum system. For that purpose, cooling water coming from the wet cooling tower of the CSP plant is used as the refrigeration source.

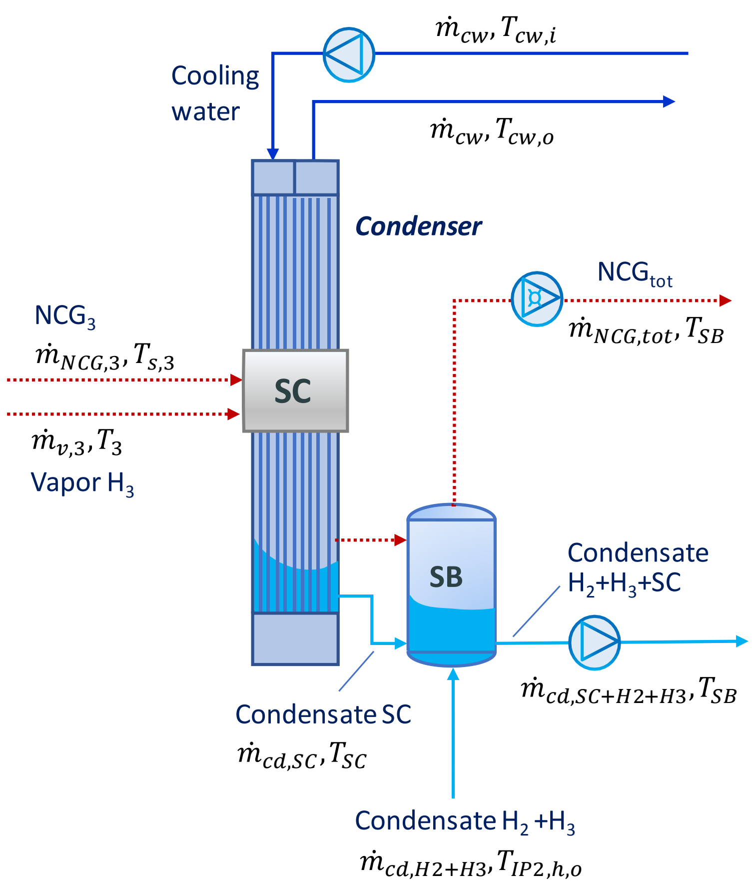

Fig. 10. Process scheme of the final condenser (SC) and separation bottle (SB).

The energy balance equation and the heat transfer equation are represented below by Eqs. (51) and (52), respectively:

$$\dot{Q}_c = \left(\dot{m}_{v,3} + \dot{m}_{NCG,3}\right)\lambda_{SC} + \left(\dot{m}_{v,3} + \dot{m}_{NCG,3}\right)\bar{c}_{p,BPE,SC}\left(T_3 - T_{SC}\right) = \dot{m}_{cw}\bar{c}_{p,cw}\left(T_{cw,o} - T_{cw,i}\right) \quad (51)$$

$$\dot{Q}_c = U_{co}A_c LMTD_c \quad (52)$$

where $\bar{c}_{p,BPE,SC}$ (J/(kg·K)) is the mean specific heat at constant pressure of condensing vapor corresponding to the BPE, T_{SC} (K) is the saturation temperature of the vapor condensing in the SC, $\dot{m}_{cw}$ (kg/s) is the mass flow rate of cooling water, $\bar{c}_{p,cw}$ (J/(kg·K)) is the mean specific heat at constant pressure of cooling water, $T_{cw,o}$ and $T_{cw,i}$ (K) are the outlet and inlet cooling water temperatures, respectively, U_{co} (W/(m^2·K)) is the overall heat transfer coefficient of the condenser based on the outer surface, A_c (m^2) is the total surface area of the tubes, and $LMTD$ (K) is the logarithmic mean temperature difference that is determined as follows:

$$LMTD_c = \frac{\Delta T_i - \Delta T_o}{ln\frac{\Delta T_i}{\Delta T_o}} = \frac{\left(T_{SC} - T_{cw,i}\right) - \left(T_{SC} - T_{cw,o}\right)}{ln\left(\frac{T_{SC} - T_{cw,i}}{T_{SC} - T_{cw,o}}\right)} \quad (53)$$

The overall heat transfer coefficient U_{co} is calculated with Eq. (54):

$$U_{co} = \frac{1}{\frac{D_{c,o}}{D_{c,i}}\frac{1}{h_{c,i}} + \frac{D_{c,o}ln(D_{c,o}/D_{c,i})}{2k_{c,w}} + \frac{1}{h_{c,o}} + R_{c,fi}} \quad (54)$$

where $R_{c,fi}$ ((m^2·K)/ W) is the internal fouling factor. The convective heat transfer coefficients, $h_{c,i}$ (W/(m^2·K)) and $h_{c,o}$ (W/(m^2·K)), have been estimated as explained in subsection 3.1.4.

The separation bottle (also represented in Fig. 10) is connected to the vacuum pump and is where the condensates from H_2 and H_3, once cooled down in PHX_2, are mixed with the condensate from the SC. The mass and energy balances applied to this component are:

$$\dot{m}_{cd,SC} + \dot{m}_{cd,H2+H3} = \dot{m}_{cd,SC+H2+H3} \tag{55}$$

$$\dot{m}_{cd,SC} h_{cd,SC} + \dot{m}_{cd,H2+H3} h_{cd,H2+H3} = \dot{m}_{cd,SC+H2+H3} h_{cd,SC+H2+H3} \tag{56}$$

where $\dot{m}_{cd,SC}$, $\dot{m}_{cd,H2+H3}$, $\dot{m}_{cd,SC+H2+H3}$ (kg/s) and $h_{cd,SC}$, $h_{cd,H2+H3}$, $h_{cd,SC+H2+H3}$ (kJ/kg) are the mass flow rates and specific enthalpies of the condensate produced in SC, the condensate coming from H_3, and the condensate exiting the SB, respectively.

3.5 Plate heat exchangers

The plate heat exchangers are used to preheat the feedwater by using part of the sensible heat content of the condensate streams H_1 and H_3 (see Fig. 1). They are modeled using the NTU-effectiveness method [22], whose equations are presented below.

$$C_h = \dot{m}_h c_{p,h} \tag{57}$$

$$C_c = \dot{m}_c c_{p,c} \tag{58}$$

$$\dot{Q}_{max} = C_{min}\left(T_{h,i} - T_{c,i}\right) \tag{59}$$

$$\epsilon = \frac{\dot{Q}}{\dot{Q}_{max}} \tag{60}$$

$$c = \frac{C_{min}}{C_{max}} \tag{61}$$

$$\dot{Q} = C_h\left(T_{h,i} - T_{h,o}\right) = C_c\left(T_{c,o} - T_{c,i}\right) \tag{62}$$

$$NTU = \frac{UA}{C_{min}} = \frac{1}{c-1} ln \frac{\epsilon - 1}{c \cdot \epsilon - 1} \tag{63}$$

where C (W/K) is the heat capacity rate, $\dot{Q}_{max}$ (W) is the maximum possible heat transfer rate, $\dot{Q}$ (W) is the actual heat transfer rate, ϵ (-) is the effectiveness, c (-) is the capacity ratio, and NTU

is the number of transfer units. Note that subscripts h and c stand for hot and cold streams, respectively.

4. Methods

4.1 Model structure

Fig. 11 shows the structure of model implementation in Modelica language [23]. The basic structuring unit in Modelica is the *class*, where the equations defining the model can be declared. In particular, the general *class* 'model' has been selected to define the equations related to each component of the plant. The effects of the MEE plant are defined by three *packages* (namely 'First effect', 'Second effect', and 'Third effect') containing three models each one, related to the outside vapor condensation ('H_i outside', with i =1,2,3), the tube wall ('H_i tube wall'), and the inside water evaporation ('H_i inside'). The rest of the components (thermocompressor, desuperheater, mixer, plate heat exchangers, separation bottle and surface condenser) are also defined using the model *class*. The main input variables, pressure and mass flow rate of motive steam (p_m, $\dot{m}_m$), temperature and mass flow rate of feed (T_f, $\dot{m}_f$), condenser pressure (p_{cond}), inlet cooling water temperature ($T_{cw,i}$), are depicted in the figure.

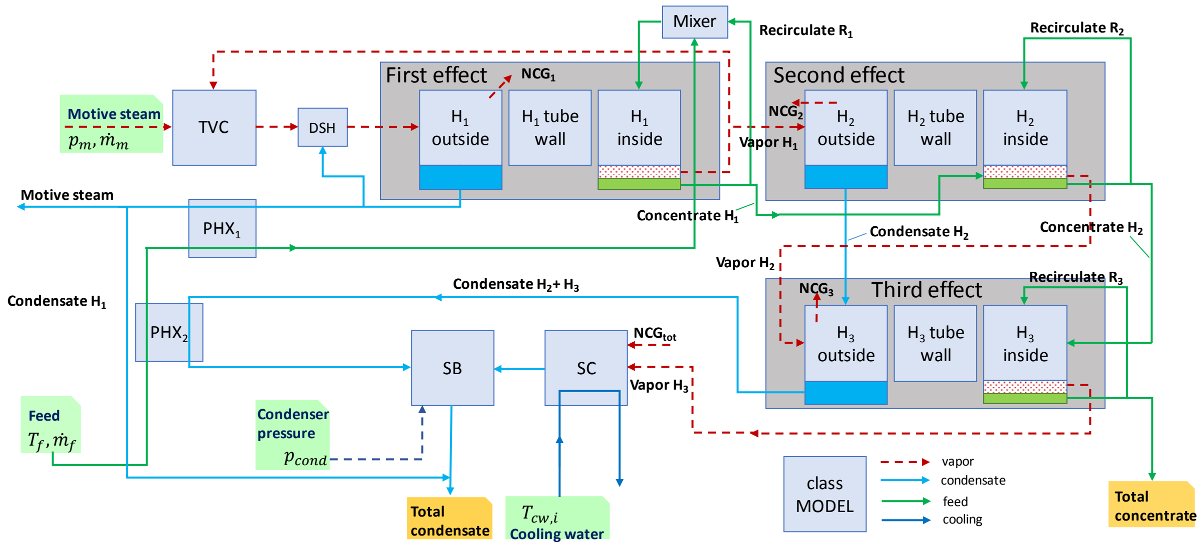

Fig. 11. Structure of model implementation in Modelica.

Modelica internally solves the set of differential equations using numerical integration methods (DASSL solver is used in this case). In the code, the solving structure of the model is hierarchical, divided into different levels, as shown in Fig. 12. It is solved starting from the top-level, named 'Solve WRS', which calls 'Solve PHX_2' (that also includes the solving of SB), which in turn calls 'Solve PHX_1' (including the call and solving of PHX_2 model), and so on. Each circle represents a model *class*, which is instantiated from the associated model 'Solve…'. The lowest level is 'Solve First Effect', which contains the models of the TVC, mixer, outside tubes, tube wall and inside tubes. In this way, the equation system of the model is closed with an equal number of equations and unknown variables.

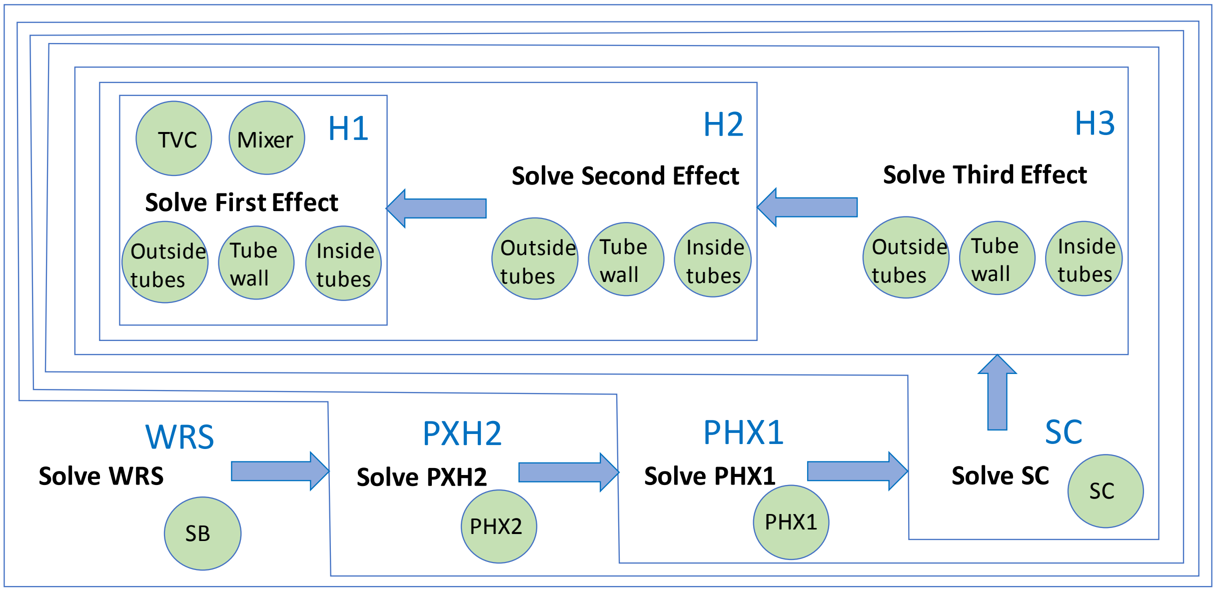

Fig. 12. Solving structure of the MEE model.

The model needs to be properly initialized because of its acausal nature. The integration period considered is 200 min to reach stationary conditions.

4.2 Evaluation of performance indexes

The performance of the WRS plant is characterized by the following indexes:

- *Gain output ratio (GOR)*: defined as the ratio of the total condensate mass flow rate produced to the motive steam mass flow rate.

$$GOR = \frac{\sum \dot{m}_{cd,i}}{\dot{m}_m} \tag{64}$$

- *Recovery ratio (RR)*: is the ratio between the total condensate flow rate produced to the feedwater flow rate.

$$RR = \frac{\sum \dot{m}_{cd,i}}{\dot{m}_f} \tag{65}$$

- *Concentration factor (CF)*: is defined as the ratio of feedwater mass flow rate to the concentrate mass flow rate.

$$CF = \frac{\dot{m}_f}{\dot{m}_c} = \frac{1}{1-RR} \tag{66}$$

- *Specific thermal energy consumption (STEC)*: defined as the ratio of the external heat added to the plant to the freshwater flow rate produced, in kWh/m^3.

$$STEC = \frac{\dot{m}_m \lambda_m}{\sum \dot{m}_{cd,i}\,/\rho_{cd}} \cdot \frac{1}{3600} \tag{67}$$

where λ_m (kJ/kg) is the specific enthalpy of condensation of the motive steam at T_m and ρ_{cd} (kg/m^3) is the density of the condensate produced at the exit of the separation bottle.

- Total power consumption required by all the pumps of the plant ($P_{W,tot}$). It is calculated with parametric equations obtained from the performance curves of the pumps (see Appendix A).

4.3 Model validation and sensitivity analysis

Firstly, the mathematical model is validated in stationary conditions due to the lack of available dynamic data, using the nominal values provided by the plant manufacturer. The inputs of the model plus the assumed parameters used are shown in Table 2. Note that the selected effectiveness of PHX_1 and PHX_2 (90.0% and 92.5%, respectively) have been determined using their technical sheets. The recirculation ratios considered are 71 t/h for effects H_1, H_2, and 53 t/h for H_3, needed to have a complete wetness in the evaporator tubes and avoid the appearance of hot spots.

Table 2. Inputs and parameters for the model validation.

Concept	Value
Motive steam mass flow rate, kg/h	2002
Motive steam pressure, bar	10.5

Feedwater temperature, °C	20
Feedwater mass flow rate, kg/h	8250
Feedwater salinity, ppm	2000
Inlet cooling water temperature, °C	33
Steam pressure in condenser, bar	0.139
Falling film velocity, m/s	0.75
NCG mass flow rate in each effect, kg/h	30
Number of tubes of H_1, H_2 and H_3, -	109, 109, 81
Length of evaporator tubes, m	8
Inner diameter of evaporator tubes, mm	50
Thickness of evaporator tubes, mm	1.5
Number of tubes of the condenser	172
Number of coolant passes	4
Inner diameter of condenser tubes, mm	27
Thickness of condenser tubes, mm	1.5
Thermal conductivity of tubes, W/(m·K)	16

After that, a sensitivity analysis of the plant performance as a function of the main operating variables (motive steam mass flow rate, feedwater mass flow rate, and final condenser pressure) is performed in dynamic conditions using the computational model. This analysis is useful for predicting how disturbances on the independent operating variables affect the water production and key efficiency parameters of the plant (STEC, RR, power consumption, concentrate salinity, etc.). The results obtained from this analysis can be relevant to identifying control strategies that allow maintaining key operational variables under suitable limits, as the concentration factor, and to operate close to the optimum points. In all the analyses, the variables that have not been modified have taken nominal condition values.

5. Results

5.1 Validation

The results of the simulation and the comparison to the design data (nominal conditions) of the plant are presented in Fig. 13. The relative error (ε) of the compared variables (mass flow rates and temperatures of the vapor/liquid at each point of the plant) is lower than 5%, which means a good approximation of the predicted values of the model to the design data. In particular, the relative errors obtained for the estimation of the mass flow rates of the total condensate and the concentrated solution are -0.04% and +0.1%, respectively. The higher discrepancies are found in the thermocompressor, in particular for the temperature of the compressed vapor (-3.7%) and the mass flow rate of suction vapor (-4%). This could be explained by the particular method followed to model this component, which is usually characterized by experimental curves, although in this work a semi-empirical curve presented by El-Dessouky et al. [19] has been used.

Table 3 shows the performance parameters obtained in the design case. It can be seen the high value of the RR (90.97%) and CF (11.08), but also the elevated thermal power required (1.1 MW), leading to a considerable specific thermal energy consumption of 147.6 kWh/m^3. However, this kind of WRS is suitable for CSP plants where waste energy from the solar field can be obtained. Usually, during the operation in conventional CSP plants, some mirrors must be defocused when the heat transfer fluid temperature exceeds its design value, for example, due to excess of direct normal irradiance. In this situation, valuable thermal energy is dumped. Therefore, instead of defocusing the mirrors, this thermal energy can be applied to power the WRS.

Table 3. Validation of the model for the design case.

Concept	Value	Model	Error (%)
GOR, -	3.74	3.75	+0.27
RR, -	90.93%	90.97%	+0.04
CF, -	11.03	11.08	+0.45
STEC, kWh/m^3	147.9	147.6	-0.20
Thermal power, kW	1116.14	1114.92	-0.11

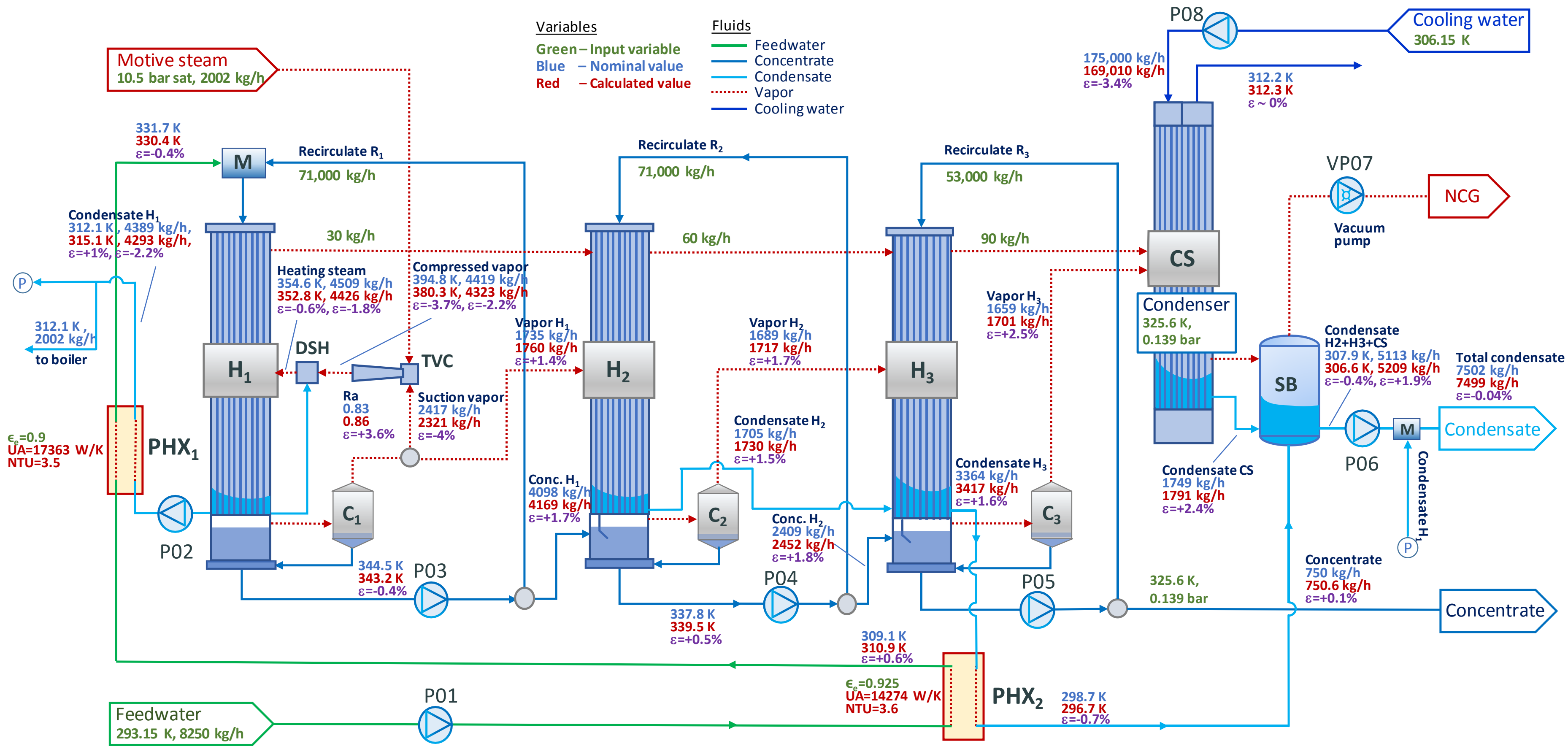

Fig. 13. Process scheme of the WRS plant with the validation of the model at nominal conditions. Feedwater, concentrate, condensate and vapor are represented by green, blue, cyan and red color lines, respectively.

5.1 Dynamic response against external disturbances

This section shows the results of the dynamic simulations that have been performed to analyze the system behavior against the presence of external disturbances on the main operational variables.

5.1.1 Motive steam mass flow rate variation

The motive steam mass flow rate is varied by ±5% with respect to its nominal value to simulate a possible disturbance in this input variable during the operation of the plant. The maximum motive steam mass flow rate increase (5%) has been selected due to the operational limits of the plant. An increment higher than 5% results in RR above 95%, which can lead to having scaling issues in the tubes of the heat exchangers, as indicated by the plant manufacturer. A ±5% step variation has been applied at t = 200 min (when all the variables are close to stationary conditions), starting from its nominal value (Fig. 14a) up to 350 min. The increment of the motive steam mass flow rate results in a similar increase (5.2%) of the water produced, from 7499.4 kg/h to 7886 kg/h (Fig. 14b), as expected, and a significant reduction of the concentrate mass flow rate (51.5%), passing from 750.6 kg/h to 364 kg/h (Fig. 14c), which in turns raises its salinity to approximately double (106.1%), from 21,990 ppm to 45,328 ppm (Fig. 14d). Notice the drastic reduction in the outlet concentrate flow rate and the consequent increase of its salinity, which lifts up far beyond the safe limit. In these conditions, the RR is 95.6%, a value that exceeds the limit provided by the plant manufacturer so that scaling issues could appear. Furthermore, it can be seen that the mass flow rates reach stationary conditions very fast while the concentrate salinity takes longer, being the dominant dynamic. The heating steam temperature and the vapor temperatures at the outlet of the evaporators (Fig. 14e) slightly increase, (2%, 1.8%, 1.5%, and 0.3% for T_{hs}, T_{H1}, T_{H2}, and T_{H3}, respectively) which leads to elevate the vapor production in the effects (Fig. 14f) by 6.3%, 6.3% and 6% for H_1, H_2 and H_3 effects, respectively. Note that the variation in T_{H3} is related to the BPE only as the condenser temperature is fixed. Finally, the cooling water requirements are higher (33.5%) when the motive steam flow rate increases due to the elevation of the flow rate of vapor to be condensed, and therefore the pumping power consumption also increases by 4.2%. The reduction of the motive steam mass flow rate by 5% has the opposite effect on the analyzed variables, being of the same magnitude in all the variables except for the outlet concentrate salinity (-34.4%) and cooling mass flow rate (-22.5%), which could be produced by the non-linearity of the associated equations.

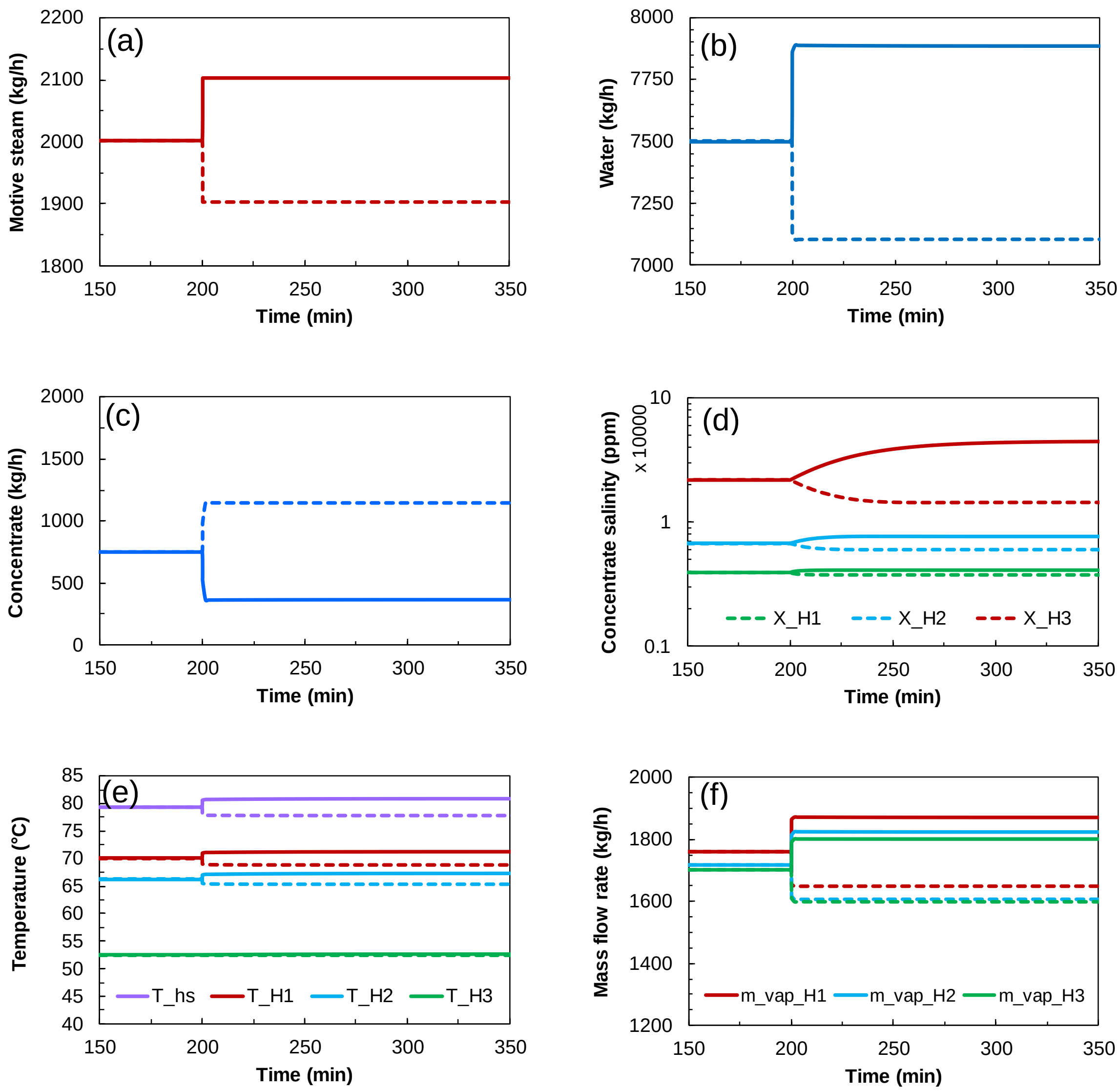

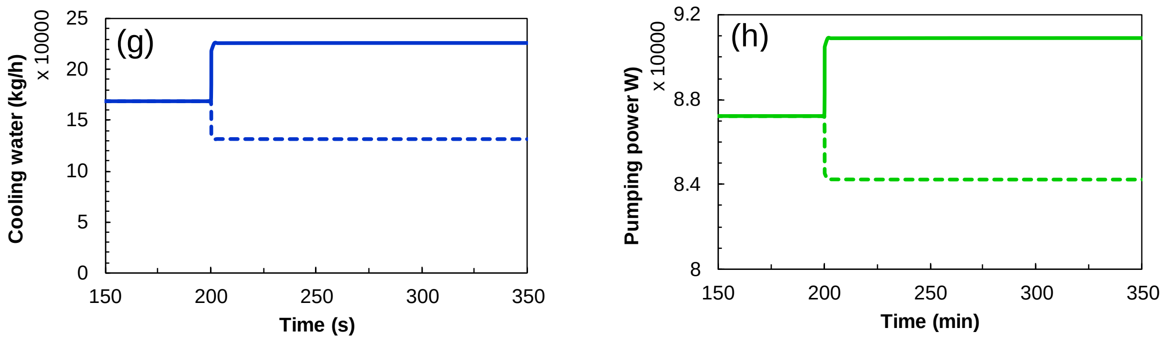

Fig. 14. Dynamic response of the plant against a ±5% step variation of the motive steam mass flow rate. The dashed line corresponds to -5% step variation. (a) Motive steam mass flow rate variation, (b) water mass flow rate produced, (c) concentrate mass flow rate, (d) concentrate salinity, (e) temperature profile, (f) mass flow rate of vapor in each effect, (g) mass flow rate of cooling water, and (h) pumping power consumption.

The influence of the motive steam mass flow rate variation in the main performance parameters of the plant is depicted in Table 4. Note that the RR has an approximately linear trend with the motive steam flow rate variation, but the CF follows roughly a quadratic tendency. The STEC is not affected.

Table 4. Main performance parameters variation with the step disturbance of the motive steam mass flow rate.

Concept	Reference	+5% $\dot{m}_m$	-5%$\dot{m}_m$
RR, -	90.9%	95.6%	86.1%
CF, -	11	22.7	7.2
STEC, kWh/m^3	148	147.8	148.4

5.1.2 Feedwater mass flow rate variation

The feedwater mass flow rate is varied between ±5% of the nominal value to investigate its effect on the key operational variables of the plant (see Fig. 15a). The lower limit is selected again considering operational aspects of the facility. An increase of the feedwater mass flow rate of 5% produces a small decrease in the water recovered of about 1% (from 7499.6 kg/h to 7427 kg/h, Fig. 15b), which may be attributed to the lower vapor production in the effects, -

1.7%, -1.6% and -1% for effects H_1, H_2 and H_3 (Fig. 15f), respectively, as a consequence of the decrease in the temperature profile of the plant, -0.3%, -0.4%, -0.3% for T_{hs}, T_{H1}, and T_{H2}, respectively (Fig. 15e). Accordingly, the outlet concentrate flow rate increases by 64.6% (Fig. 15c), leading to a decrease in its salinity (-36.2%), as depicted in Fig. 15d. Also, the cooling mass flow rate has a reduction of -4.1% (Fig. 15g) due to the lower amount of vapor to be condensed, and therefore the pumping power requirement is slightly lower (-0.5%, Fig. 15h).

The decrease of the feedwater mass flow rate by 5% has opposite effects on the variables analyzed, with a trend nearly symmetric. The water production is slightly increased to 7566 kg/h (0.9%). One relevant result here is related to the salinity of the outlet concentrate, which is increased from 21,990 ppm to 57,777 ppm, i.e., a rise of 163%, resulting in a RR of 96.5%, a value that could lead to having scaling issues.

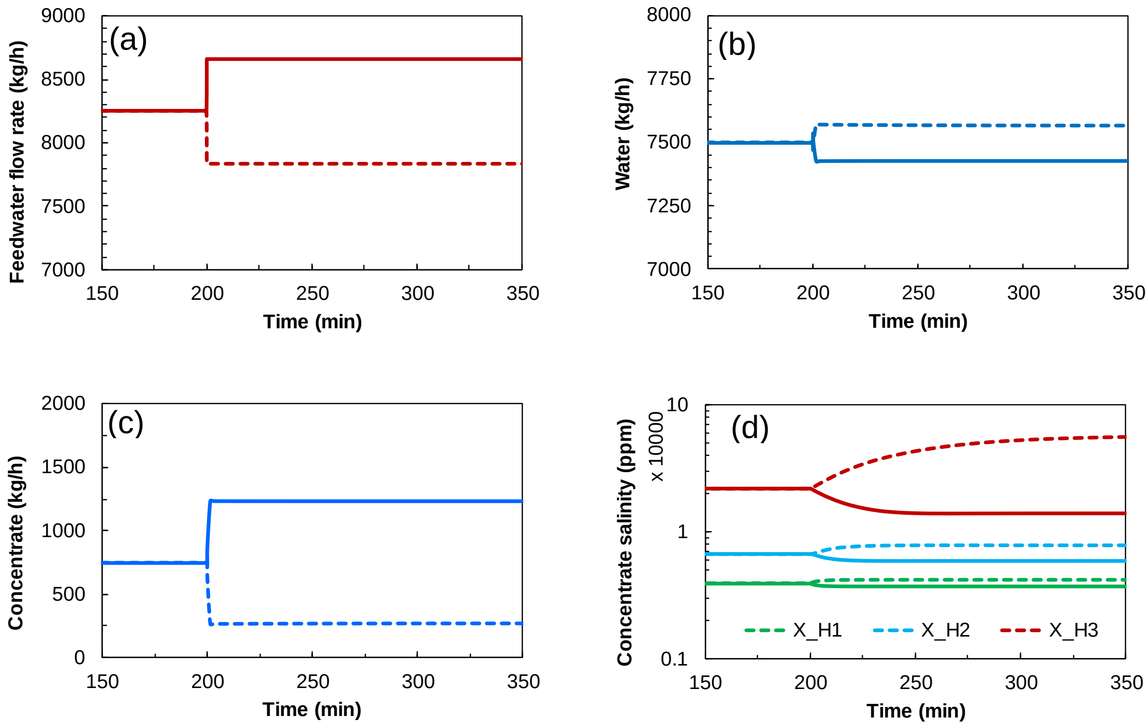

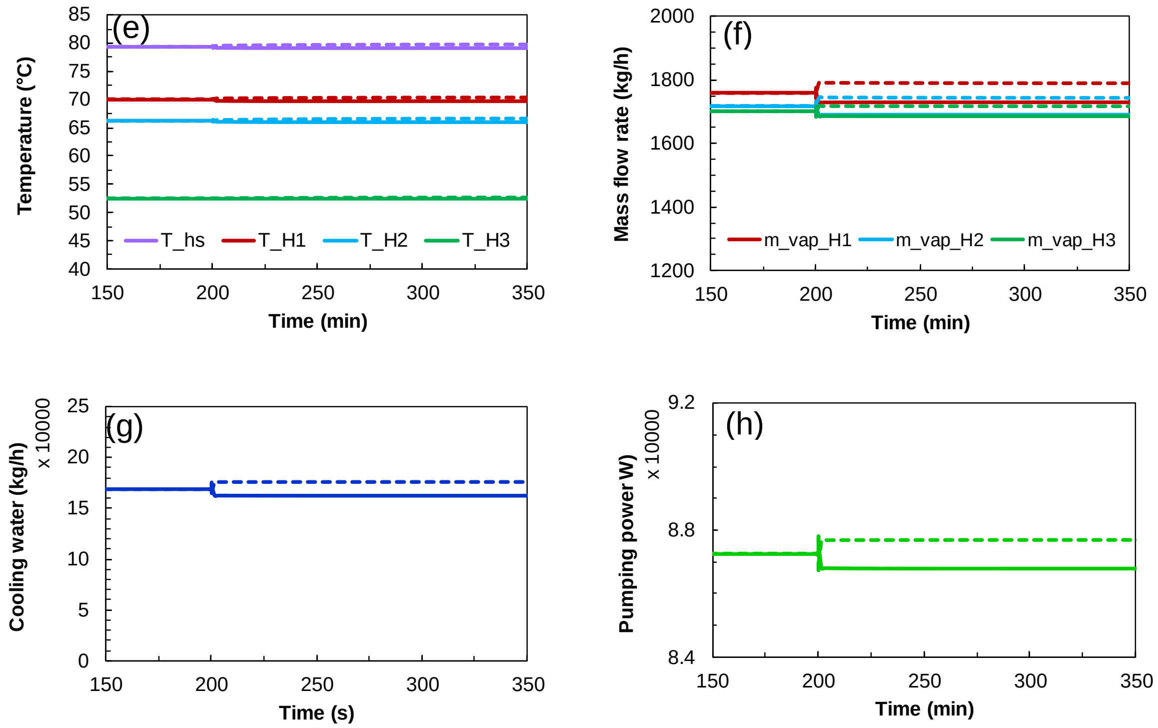

Fig. 15. Dynamic response of the plant against a ±5% step variation of the feedwater mass flow rate. The dashed line corresponds to -5% step variation. (a) Feedwater mass flow rate variation, (b) water mass flow rate produced, (c) concentrate mass flow rate, (d) concentrate salinity, (e) temperature profile, (f) mass flow rate of vapor in each effect, (g) mass flow rate of cooling water, and (h) pumping power consumption.

Table 5 shows the effect of the feedwater mass flow rate variation on the key performance parameters of the plant. It can be seen how reducing the feedwater mass flow rate produces a similar effect as increasing the motive steam mass flow rate, with a high value of the RR (unsafe zone, >95%) and CF, while the STEC is only marginally affected by this variation.

Table 5. Main performance parameters variation with the step disturbance of the feedwater mass flow rate.

Concept	Reference	+5% $\dot{m}_f$	-5%$\dot{m}_f$
RR, -	90.9%	85.7%	96.5%
CF, -	11	7	28.9
STEC, kWh/m^3	148	149.4	146.7

5.1.3 Condenser pressure variation

The pressure in the SC is varied (Fig. 16a) by increasing it from the nominal value, 139 mbar, to 500 mbar (only the increase of pressure is analyzed because the nominal value is the lowest one achieved by the vacuum pump). This increment is equivalent to lifting the saturation temperature from 52.6 °C to 81.6 °C, which is a very extreme case. Results obtained show a moderate decrease of the water production (Fig. 16b) from 7499.4 to 6809.7 kg/h (-9.2%) and a significant increment of the concentrate mass flow rate, which pass from 750.6 kg/h to 1440.3 kg/h (91.9%), Fig. 16c. Therefore, the outlet concentrate salinity is decreased by half, from 21,990 to 11,456 ppm (-48%, Fig. 16d). This may be explained by the decrease in the temperature difference between effects. Even though the temperature profile of the plant is shifted and risen, passing T_{hs} T_{H1}, T_{H2}, and T_{H3} from 79.4 °C, 70 °C, 66.3 °C and 52.4 °C to 104.5 °C, 96.1 °C, 93 °C and 81.4 °C, respectively, the total temperature jump in the plant is lower (from 27 °C to 23 °C) (see Fig. 16e). As a result, lower vapor production is achieved in each effect, as can be seen in Fig. 16f, with a decrease of -11.3%, -11.5% and -11.1% for H_1, H_2 and H_3 effects, respectively. The cooling mass flow rate required in the condenser, Fig. 16g, highly decreases from 169,010 kg/h to 20,035 kg/h (-88.1%) because of the lower amount of vapor to be condensed and the larger temperature increase of the cooling water, which is risen from 6 °C to 44 °C. As a result, the pumping power consumption is also decreased (Fig. 16h) by 16%, passing from 87.2 kW to 73.3 kW.

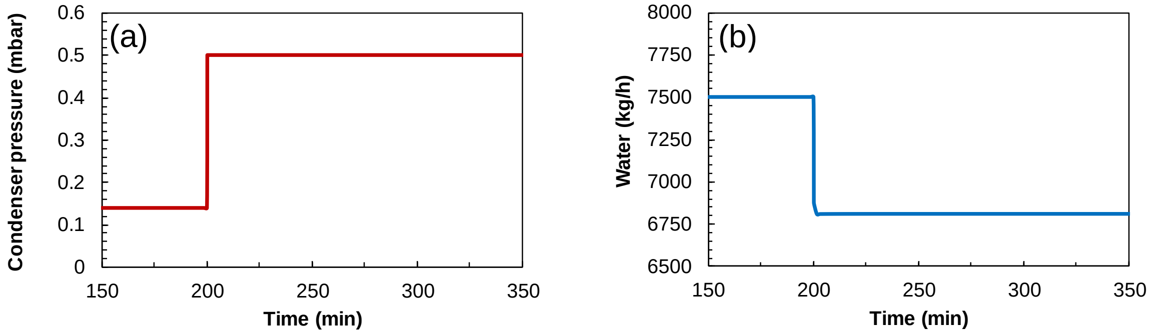

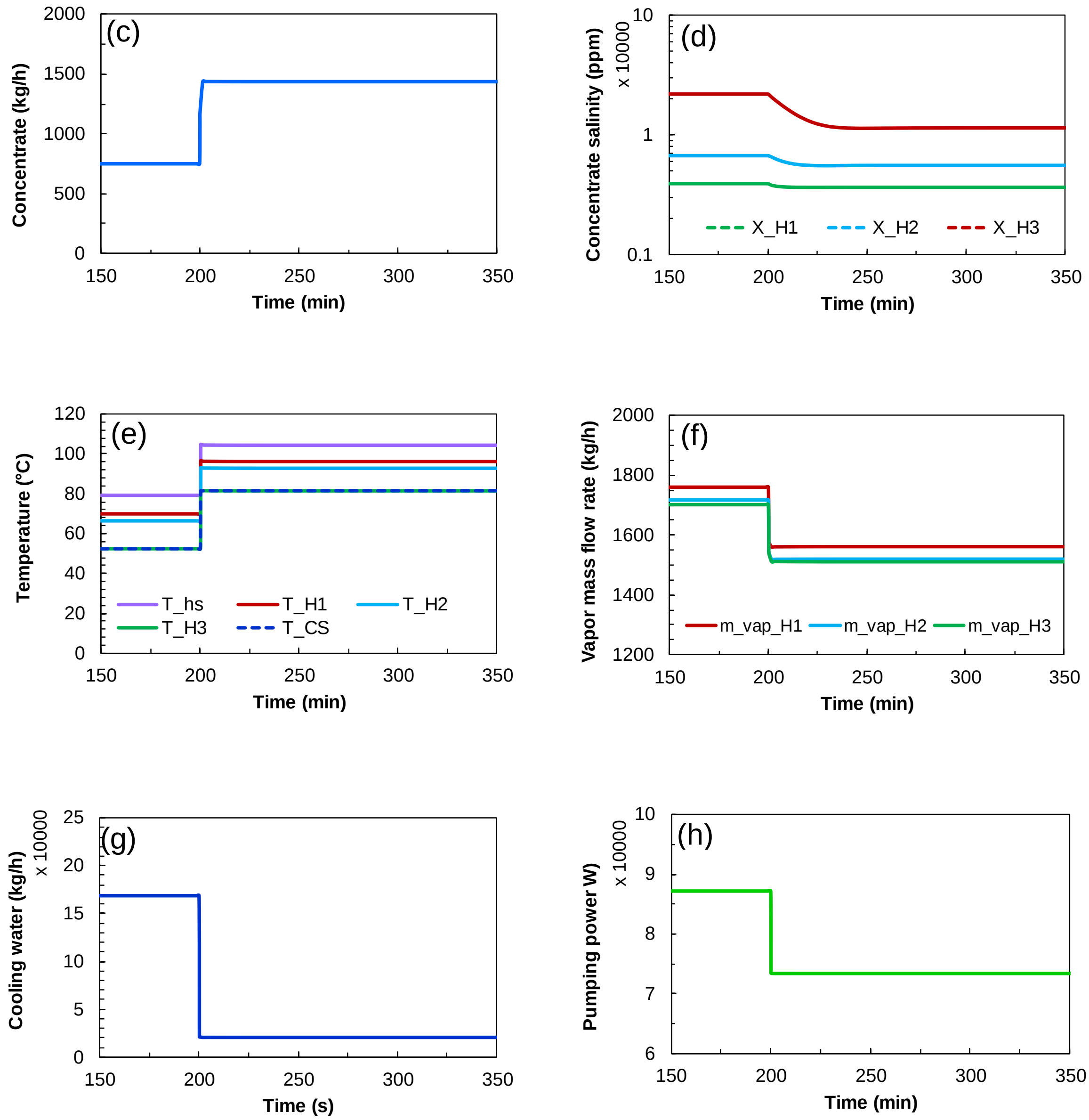

Fig. 16. Dynamic response of the plant against an increase of the condenser pressure. (a) Condenser pressure variation, (b) water mass flow rate produced, (c) concentrate mass flow rate, (d) concentrate salinity, (e) temperature profile, (f) mass flow rate of vapor in each effect, (g) mass flow rate of cooling water, and (h) pumping power consumption.

The influence of increasing the condenser pressure on the RR, CF and STEC is depicted in Table 6. It is shown how both RR and CF are in a safe operation zone, with lower values than the nominal case, while the STEC is slightly increased due to the reduction of water produced while maintaining the same heat rate consumption.

Table 6. Main performance parameters variation with the step disturbance of the condenser pressure.

Concept	Reference	$p_{cond} = 500$ mbar
RR, -	90.9%	82.5%
CF, -	11	5.7
STEC, kWh/m^3	148	162.3

5.1.4 Simultaneous variation of the motive steam and feedwater mass flow rate

As it has been shown in subsection 5.1.1, increasing the motive steam mass flow rate improves the water production, but also it could lead to severe scaling issues and the shutdown of the plant due to the increase of the concentrate salinity. The same happens when the feedwater mass flow rate is decreased (subsection 5.1.2). Therefore, it is important to implement control strategies able to maintain the salinity of the concentrate under safe limits when the motive steam increases or the feedwater flow rate decreases.

One possible strategy to maintain the concentrate salinity could be to increase/decrease at the same time both the motive steam mass flow rate and the feedwater mass flow rate in the same proportion, so the evaporation ratio could be kept similar to that of the design conditions (see Fig. 17a). In this case, it can be seen how the concentrate salinity is kept near the initial nominal value, 21,990 ppm, when a disturbance in the plant produces a +5% variation of the motive steam mass flow rate or a -5% variation of the feedwater mass flow rate. In the first case, by also applying an increment of 5% to the feedwater mass flow rate, the salinity is reduced from 45,323 ppm to 20,481 ppm (45.3%), while in the second case, decreasing the motive steam mass flow rate by 5% leads to a reduction of the salinity from 57,752 ppm to 23,767 ppm (41.2%). The effect of this simultaneous variation on the water production, and its comparison with the individual variations of the motive steam (+5%) and feedwater (-5%) mass flow rates, are presented in Fig. 17b. In the first case, the water production is still higher than the nominal case (4.2% of increase), 7817 kg/h against 7499 kg/h, although lower than the case where only the motive steam flow rate is increased (7886 kg/h, but operating in an unsafe zone due to the increased concentrate salinity). In the second case, the water production is reduced from its nominal value to 7178 kg/h (4.3% of reduction), which is lower than the standalone decrease of the feedwater flow rate (7566 kg/h, but again operating in an unsafe zone). This is expected due to the lower thermal energy introduced in the system.

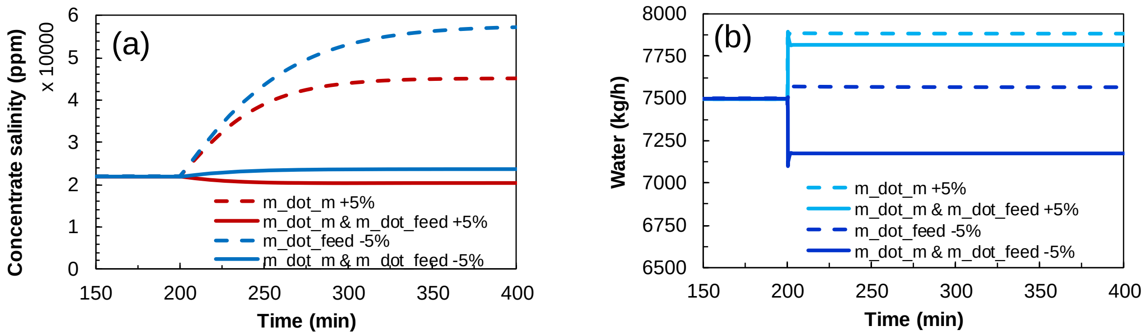

Fig. 17. Dynamic response of the (a) concentrate salinity and (b) water production against a simultaneous variation (continuous lines, ±5%) of motive steam and feedwater mass flow rates. It is also shown the comparison with the individual variations (discontinuous lines, +5% motive steam and -5% feedwater mass flow rates).

6. Conclusions

A dynamic model for a vertical MEE plant to be used for water recovery purposes in a CSP plant has been developed and presented in detail. The set of equations used for every component of the plant has been described, together with all the relationships needed to close the model. It has been simulated under nominal conditions in order to be validated against the design data provided by the plant manufacturer, showing a good agreement for all the variables (relative errors lower than 5%).

After validation, the model has been used to perform a sensitivity analysis at dynamic conditions to identify the operating conditions leading to the maximum water production and the possible unfeasible operation points of the plant. Particularly, from the sensitivity analysis, it was observed that an increase of the motive steam mass flow rate of 5% leads to an increase in the water production of 5.2% but also to a high increase of the concentrate salinity (106%), which may cause severe scaling in the evaporator tubes. A similar effect occurs when the feedwater flow rate is decreased by 5%. The water production is marginally increased by ~1%, but the concentrate salinity is raised by 163%, hence operating in an unsafe zone. These problems could be solved by implementing a control strategy consisting in varying the motive steam and feedwater mass flow rates simultaneously at the same proportion, in such a way that the outlet salinity can be maintained under a feasible operating range. As an example, a simultaneous increase (+5%) and decrease (-5%) of the motive and feedwater mass flow rates has been performed, obtaining a concentrate salinity of 20,481 ppm and 23,767 ppm, respectively, which are near to the nominal value, 21,990 ppm. In the first case, the water production is improved by 4.2% with respect the nominal value. Also, model predictions showed that the increase in the condenser pressure up to 500 mbar worsens the water production by ~9% although decreases the pumping power consumption up to 16%.

The results obtained prove the potential of the presented model as a tool to simulate the dynamic behavior of this kind of plant, aiming to predict the optimal operating conditions that lead to the maximum water production and the minimum energetic consumption. These plants can be an opportunity to reduce the water consumption in CSP by the reuse of the wastewater streams.

Nomenclature

Acronyms and abbreviations

BPE	Boiling Point Elevation
CF	Concentration Factor
CSP	Concentrating Solar Power

CV	Control Volume
DSH	DeSuperHeater
GOR	Gain Output Ratio
LMTD	Logarithmic Mean Temperature Difference
MEE	Multi-Effect Evaporator
NCG	Non-Condensable Gases
NEA	Non-Equilibrium Allowance
NTU	Number of Transfer Units
OHTC	Overall Heat Transfer Coefficient
PHX	Plate Heat eXchanger
RR	Recovery Ratio
SB	Separation Bottle
SC	Surface Condenser
STEC	Specific Thermal Energy Consumption
TVC	Thermal Vapor Compression
VP	Vacuum Pump
WRS	Water Recovery System

Variables

A	Area, m^2
A_c	Area of the falling film crown, m^2
C	Heat capacity rate, kW/K
c	Capacity ratio, -
$\bar{c}_p$	Average specific heat at constant pressure, kJ/(kg·K)
D	Diameter, m
E	Internal energy, kJ
h	Specific enthalpy, kJ/kg or convective heat transfer coefficient, kW/(m^2·K)
k	Thermal conductivity, W/(m·K)
L	Length of the tube, m, or level of liquid, m
$LMTD$	Logarithmic mean temperature difference, K
M	Mass of falling film, kg
$\dot{m}$	Mass flow rate, kg/s
N_{av}	Average value of generic variable
N_t	Number of tubes, -
NEA	Non-equilibrium allowance, K
NTU	Number of transfer units, -
P_W	Power, kW
p	Pressure, Pa
Pr	Film Prantdl number,-
$\dot{Q}$	Heat rate, kW

Ra	Entrainment ratio, -
Re	Film Reynolds number
R_f	Fouling factor, $(m^2·K)/kW$
R	Thermal resistance, K/W, or radius, m
T	Temperature, K
U_i	Overall heat transfer coefficient referred to the internal area, $kW/(m^2·K)$
v	Velocity of the falling film, m/s
X	Salinity, ppm

Greek letters

ϵ	Effectiveness, -
ε	Relative error (%)
λ	Specific enthalpy of vaporization/condensation, kJ/kg
μ	Dynamic viscosity, $(N·s)/m^2$
ρ	Density, kg/m^3
τ	Residence time of the falling film, s

Subscripts

av	Average
c	Concentrate or cold fluid
cd	Condensate
$comp$	Compressed
$cond$	Condenser
cv	Convection
cw	Cooling water
dsh	Desuperheater
ev	Evaporation
f	Feedwater
fl	Flash
h	Hot fluid
i	Inlet/inside
is	inlet subcooled
L	Liquid
M	Mixer
m	Motive steam
NCG	Non-condensable gases
o	Outlet/outside
Hi	Effect Hi
r	Recirculate
S	Tube outer vapor
SC	Surface condenser
sat	Saturated
sen	Sensible

sh	Desuperheater
suc	Suction steam
tot	Total
tr	Conduction
v, V	Vapor
w	Tube wall

Acknowledgements

The authors would like to acknowledge the E. U. through the H2020 Program for the financial support of this work under the SOLWARIS project with contract number 792103.

References

[1] SOLWARIS. https://solwaris.eu/

[2] J.A. Carballo, J. Bonilla, L. Roca, A. De la Calle, P. Palenzuela, D.C. Alarcón-Padilla, Optimal operating conditions analysis for a multi-effect distillation plant according to energetic and exergetic criteria., Desalination. 435 (2018) 70–76. https://doi.org/10.1016/j.desal.2017.12.013.

[3] S. Angeletti, M. Moresi, Modelling of multiple-effect falling-film evaporators, Int. J. Food Sci. Technol. 18 (1983) 539–563. https://doi.org/10.1111/j.1365-2621.1983.tb00296.x.

[4] M.H. Khademi, M.R. Rahimpour, A. Jahanmiri, Simulation and optimization of a six-effect evaporator in a desalination process, Chem. Eng. Process. Process Intensif. 48 (2009) 339–347. https://doi.org/10.1016/j.cep.2008.04.013.

[5] S. Khanam, B. Mohanty, Development of a new model for multiple effect evaporator system, Comput. Chem. Eng. 35 (2011) 1983–1993. https://doi.org/10.1016/j.compchemeng.2010.11.001.

[6] D. Srivastava, B. Mohanty, R. Bhargava, Modeling and simulation of MEE system under fouling condition, Int. J. Eng. Res. Technol. 2 (2013) 2333–2340. www.ijert.org.

[7] M. Sagharichiha, A. Jafarian, M. Asgari, R. Kouhikamali, Simulation of a forward feed multiple effect desalination plant with vertical tube evaporators, Chem. Eng. Process.

Process Intensif. 75 (2014) 110–118. https://doi.org/10.1016/j.cep.2013.11.008.

[8] H. Andre, R.A. Ritter, Dynamic response of a double effect evaporator, Can. J. Chem. Eng. 46 (1968) 259–264. https://doi.org/10.1002/cjce.5450460409.

[9] P. Quaak, M.P.C.M. van Wijck, J.J. van Haren, Comparison of process identification and physical modelling for falling-film evaporators, Food Control. 5 (1994) 73–82. https://doi.org/10.1016/0956-7135(94)90089-2.

[10] J.A. Winchester, C. Marsh, Dynamics and control of falling film evaporators with mechanical vapour recompression, Chem. Eng. Res. Des. 77 (1999) 357–371. https://doi.org/10.1205/026387699526340.

[11] Z. Stefanov, K.A. Hoo, A distributed-parameter model of black liquor falling film evaporators. Part I. Modeling of a single plate, Ind. Eng. Chem. Res. 42 (2003) 1925–1937. https://doi.org/10.1021/ie020483a.

[12] Z.I. Stefanov, K.A. Hoo, Distributed parameter model of black liquor falling-film evaporators. 2. Modeling of a multiple-effect evaporator plant, Ind. Eng. Chem. Res. 43 (2004) 8117–8132. https://doi.org/10.1021/ie049611g.

[13] D. Kumar, V. Kumar, V.P. Singh, Modeling and dynamic simulation of mixed feed multi-effect evaporators in paper industry, Appl. Math. Model. 37 (2013) 384–397. https://doi.org/10.1016/j.apm.2012.02.039.

[14] F. Medhat Bojnourd, M.A. Fanaei, H. Zohreie, Mathematical modelling and dynamic simulation of multi-effect falling-film evaporator for milk powder production, Math. Comput. Model. Dyn. Syst. 21 (2015) 336–358. https://doi.org/10.1080/13873954.2014.980276.

[15] Dymola 2020x — Dynamic Modeling Laboratory, (2020). www.3ds.com.

[16] J.A. Shmerler, I. Mudawwar, Local evaporative heat transfer coefficient in turbulent free-falling liquid films, Int. J. Heat Mass Transf. 31 (1988) 731–742. https://doi.org/10.1016/0017-9310(88)90131-7.

[17] D.A. Labuntsov, Heat Transfer in Film Condensation of Pure Vapors on Vertical Surfaces and Horizontal Tubes, Teploenergetika. 4 (1957) 72–79.

[18] A. Cipollina, M. Agnello, A. Piacentino, A. Tamburini, B. Ortega, P. Palenzuela, D. Alarcon, G. Micale, A dynamic model for MED-TVC transient operation,

Desalination. 413 (2017) 234–257. https://doi.org/10.1016/j.desal.2017.03.005.

[19] H. El-Dessouky, Modeling and simulation of thermal vapor compression desalination plant, Symp. Desalin. Seawater with Nucl. Energy. (1997).

[20] A.S. Hassan, M.A. Darwish, Performance of thermal vapor compression, Desalination. 335 (2014) 41–46. https://doi.org/10.1016/j.desal.2013.12.004.

[21] O. Miyatake, K. Murakami, Y. Kawata, T. Fujii, Fundamental experiments with flash evaporation, Heat Transf. Jpn. Res. 2 (1973) 89–100.

[22] W.M. Kays, A.L. London, Compact heat exchangers, 2d ed., McGraw-Hill, New York, 1964.

[23] Modelica Language — Modelica Association, (n.d.). https://modelica.org/modelicalanguage.html (accessed June 11, 2021).

[24] M.H. Chun, K.T. Kim, Assessment of the new and existing correlations for laminar and turbulent film condensations on a vertical surface, Int. Commun. Heat Mass Transf. 17 (1990) 431–441. https://doi.org/10.1016/0735-1933(90)90062-O.

[25] V. Guichet, S. Almahmoud, H. Jouhara, Nucleate pool boiling heat transfer in wickless heat pipes (two-phase closed thermosyphons): A critical review of correlations, Therm. Sci. Eng. Prog. 13 (2019). https://doi.org/10.1016/j.tsep.2019.100384.

[26] V. Gnielinski, New equations for heat and mass transfer in turbulent pipe and channel flow, Int. Chem. Eng. 16 (1976) 359–368.

[27] M.H. Sharqawy, J.H. Lienhard V, S.M. Zubair, Thermophysical properties of seawater: A review of existing correlations and data, Desalin. Water Treat. 16 (2010) 354–380. https://doi.org/http://dx.doi.org/10.5004/dwt.2010.1079.

Appendix A

A1. Heat transfer coefficients

For the external steam condensation (assumed to be in wavy regime) the heat transfer coefficient h_o (kW/(m^2·K)) correlation selected is the one presented by Labuntsov [17], who developed the following empirical correlation for the film condensation average heat transfer coefficient in the laminar-wavy regime (30 < Re_L< 1600) [24]:

$$h_o^* = 1.39 \cdot Re_L^{-0.29} \quad \text{(A.1)}$$

where Re_L is the film Reynolds number, defined as:

$$Re_L = \frac{4\Gamma}{\mu_L} = \frac{4\dot{m}}{P\mu_L} = \frac{\dot{m}}{\pi D_o \mu_L} \quad \text{(A.2)}$$

where Γ (kg/(m·s)) is the mass flow rate per unit periphery, P (m) is the wetted perimeter, $\dot{m}$ (kg/s) is the mass flow rate of inlet falling film in the case of internal evaporation or the mass flow rate of condensate in the case of external condensation, D_o (m) is the outer tube diameter, and μ_L ((N·s)/m^2) is the dynamic viscosity of the liquid.

The heat transfer coefficient h_i (kW/(m^2·K)) for the internal falling film evaporation (considered to be in turbulent regime) selected is the one from Shmerler & Mudawwar [16], which is one of the correlations recommended by Guichet et al. [25]. The correlation estimates the heat transfer coefficient in evaporative turbulent free-falling films with 4990 < Re_L< 37,620 and 1.75 < Pr_L < 5.42.

$$h_i^* = 3.8 \times 10^{-3} Re_L^{0.35} Pr_L^{0.95} \quad \text{(A.3)}$$

where Pr_L is the film Prandtl number, defined as:

$$Pr_L = \frac{\mu_L c_{pL}}{k_{TL}} \quad \text{(A.4)}$$

where c_{pL} (J/(kg·K)) is the specific heat at constant pressure of the liquid, and k_{TL} (W/(m·K)) is the thermal conductivity of the liquid.

For the coolant heating inside the tubes of the condenser, the correlation presented by Gnielinski [26] for fully developed turbulent flow in circular tubes with constant heat flux has been used, valid for 2300 < Re_L< 5×10^6, and 0.5 < Pr_L < 2000:

$$h_i = Nu \cdot \frac{k_{TL}}{D_i} \quad \text{(A.5)}$$

$$Nu = \frac{(f/2)(Re_L - 1000)Pr_L}{1 + 12.7(f/2)^{1/2}\left(Pr_L^{2/3} - 1\right)} \tag{A.6}$$

where Nu is the Nusselt number, D_i (m) is the tube inner diameter, and the factor f can be calculated with:

$$f = (1.58 \ln Re_L - 3.28)^{-2} \tag{A.7}$$

A2. Thermophysical properties

The boiling point elevation is calculated with Eq. (A.8) [27]:

$$BPE = A \cdot s^2 + B \cdot s \tag{A.8}$$

where s (kg/kg) is the salinity and coefficients A and B are defined as:

$$A = -4.584 \times 10^{-4} \cdot t^2 + 2.823 \times 10^{-1} \cdot t + 17.95 \tag{A.9}$$

$$B = 1.536 \times 10^{-4} \cdot t^2 + 5.267 \times 10^{-2} \cdot t + 6.56 \tag{A.10}$$

with t (°C) the temperature in Celsius.

A3. Power consumption correlations of the pumps

Pumping power correlations have been obtained from the technical specification's sheets of the pumps.

$$P_{W1/2/6} = 72.131\,\dot{V}_x + 1293.4 \tag{A.11}$$

$$P_{W3/4/5} = -0.11806\,\dot{V}_x^2 + 48.750\dot{V}_x + 6400 \tag{A.12}$$

$$P_{W7} = 1.1085 \times 10^{-5} p_{SC}^3 - 2.3286 \times 10^{-2} p_{SC}^2 + 13.307 p_{SC} + 4804.3 \tag{A.13}$$

$$P_{W8} = -0.1703\,\dot{V}_x^2 + 131.5\,\dot{V}_x + 30860 \tag{A.14}$$

where $\dot{V}_x$ (m^3/h) is the volumetric flow rate passing through the corresponding pump x.

Figure

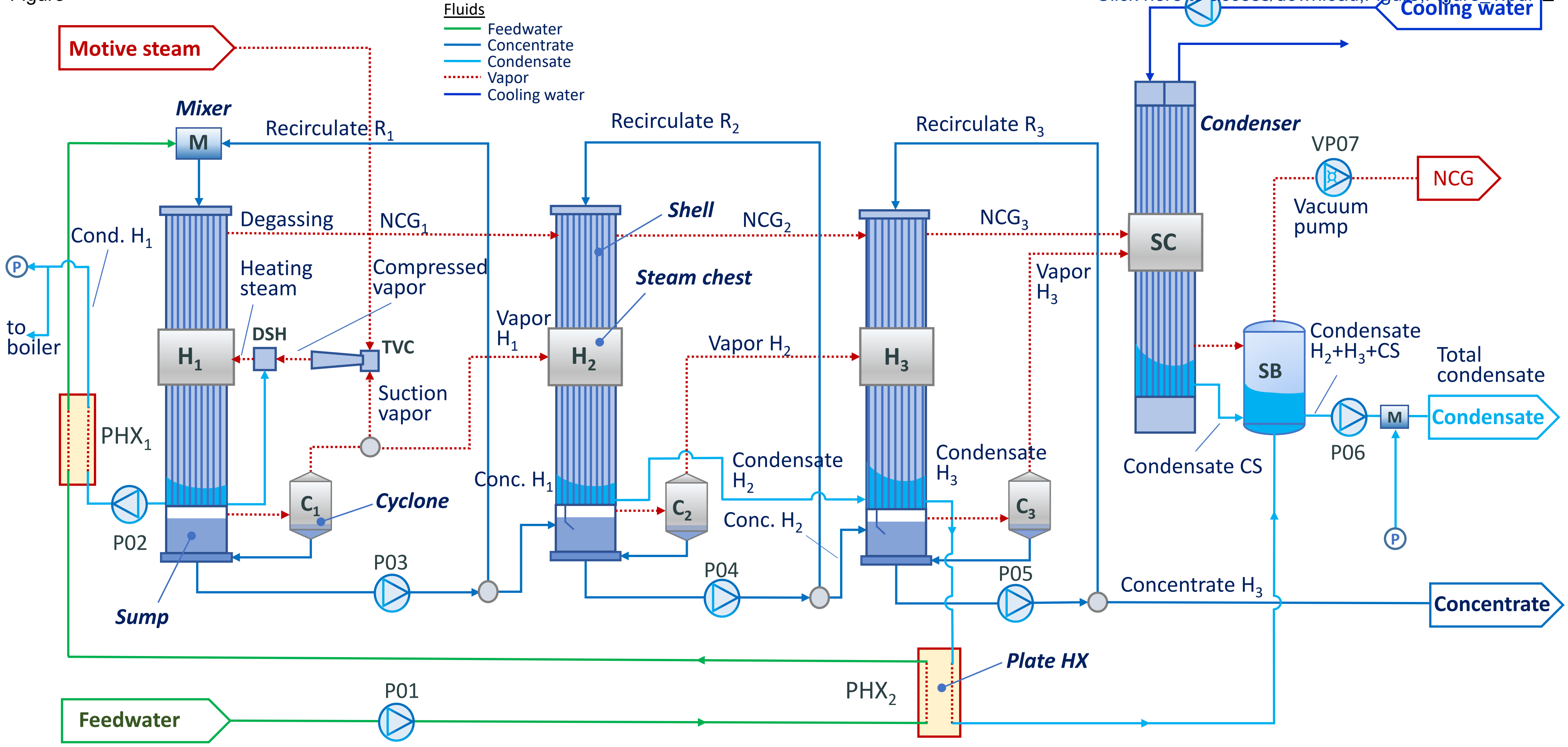

Fluids
Feedwater
Concentrate
Condensate
Vapor
Cooling water
Motive steam
Mixer
M
Recirculate R_1
Recirculate R_2
Recirculate R_3
Degassing
NCG_1
NCG_2
NCG_3
Cond. H_1
Heating steam
Compressed vapor
DSH
TVC
Suction vapor
H_1
H_2
H_3
Shell
Steam chest
Vapor H_1
Vapor H_2
Vapor H_3
P
to boiler
PHX_1
P02
C_1
C_2
C_3
Cyclone
Sump
P03
Conc. H_1
Conc. H_2
Condensate H_2
Condensate H_3
P04
P05
Concentrate H_3
P08
Cooling water
Condenser
SC
VP07
Vacuum pump
NCG
SB
Condensate H_2+H_3+CS
Total condensate
Condensate CS
P06
M
Condensate
P
Concentrate
Plate HX
PHX_2
P01
Feedwater

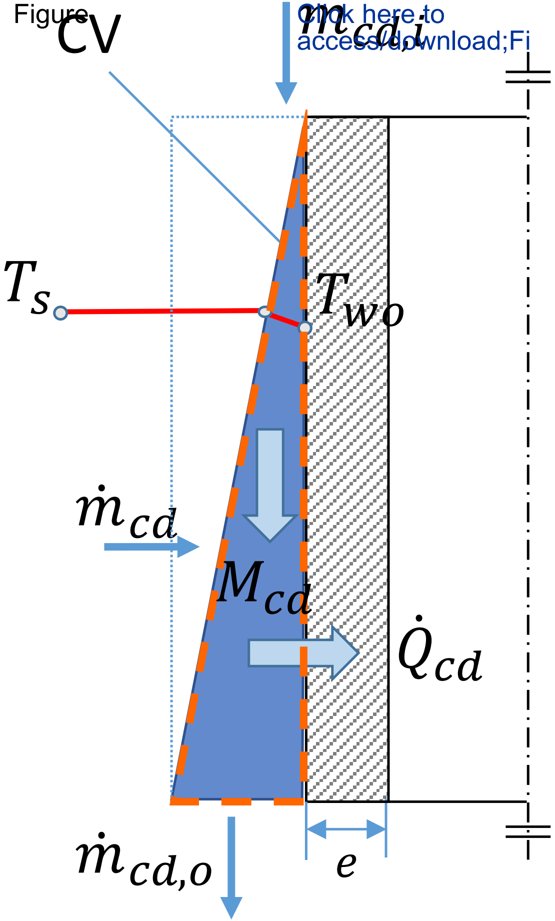
CV
$\dot{m}_{cd,i}$
T_s
T_{wo}
$\dot{m}_{cd}$
M_{cd}
$\dot{Q}_{cd}$
$\dot{m}_{cd,o}$
e

Figure

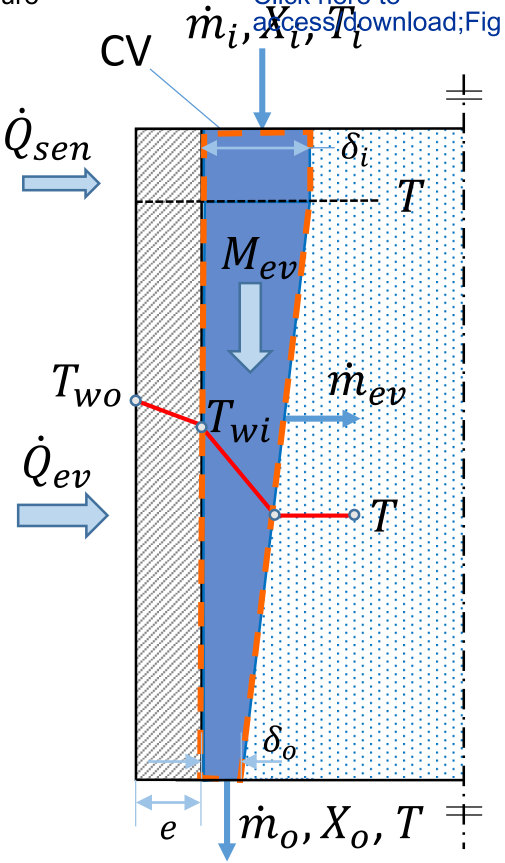

$\dot{m}_i, X_i, T_i$
CV
$\dot{Q}_{sen}$
δ_i
T
M_{ev}
T_{wo}
$\dot{m}_{ev}$
T_{wi}
$\dot{Q}_{ev}$
T
δ_o
e
$\dot{m}_o, X_o, T$

Figure

Click here to access/download;Figure;Figure_4.pdf

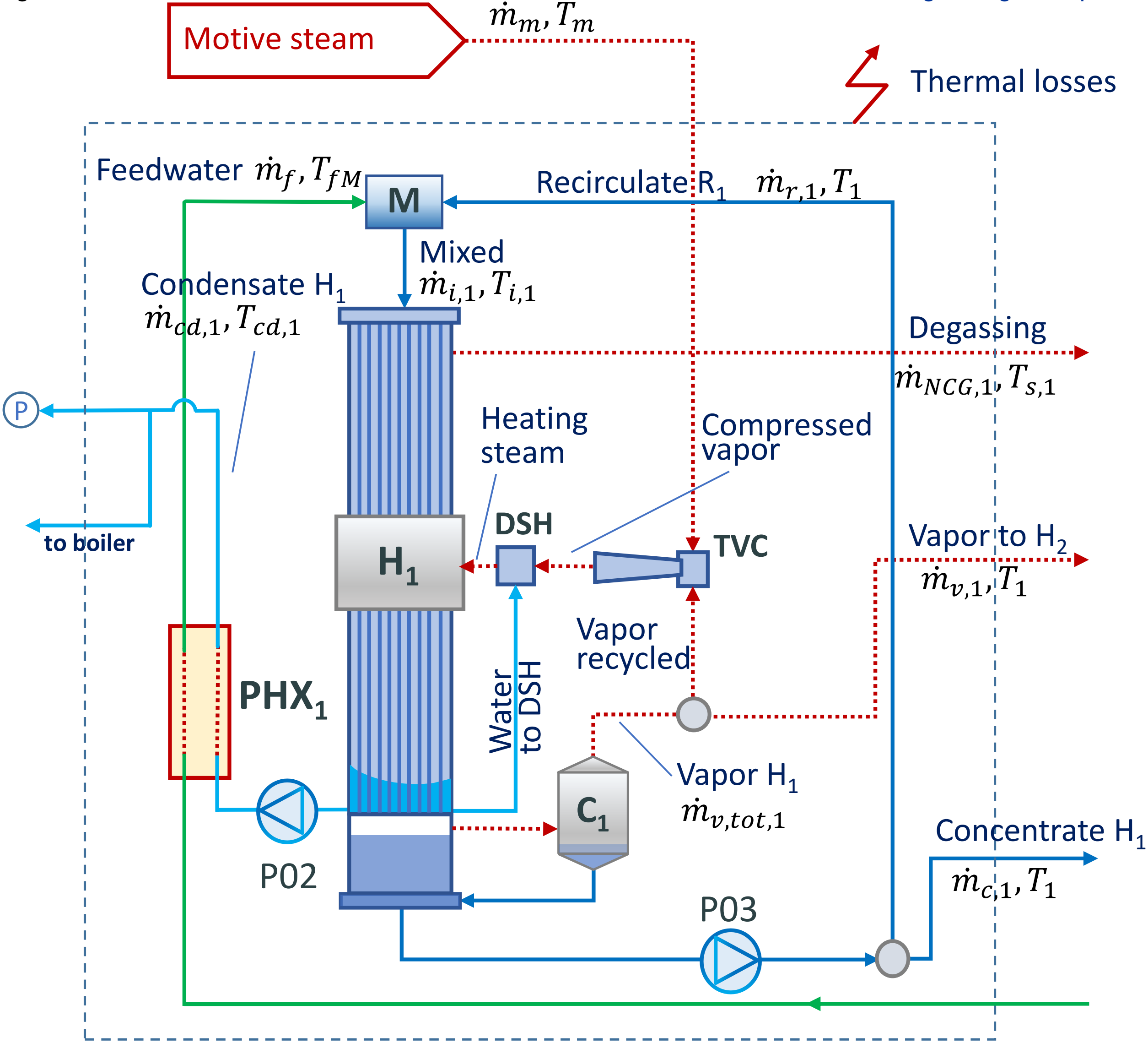

Figure

Click here to access/download;Figure;Figure_5.pdf

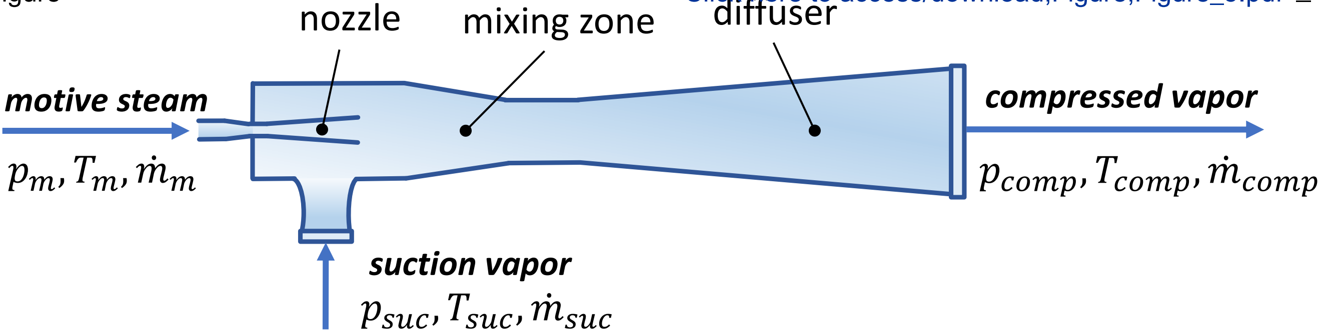

Figure

Click here to access/download;Figure;Figure_6.pdf

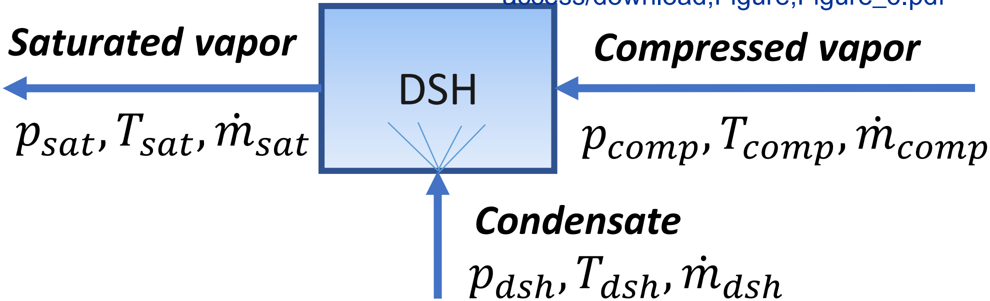

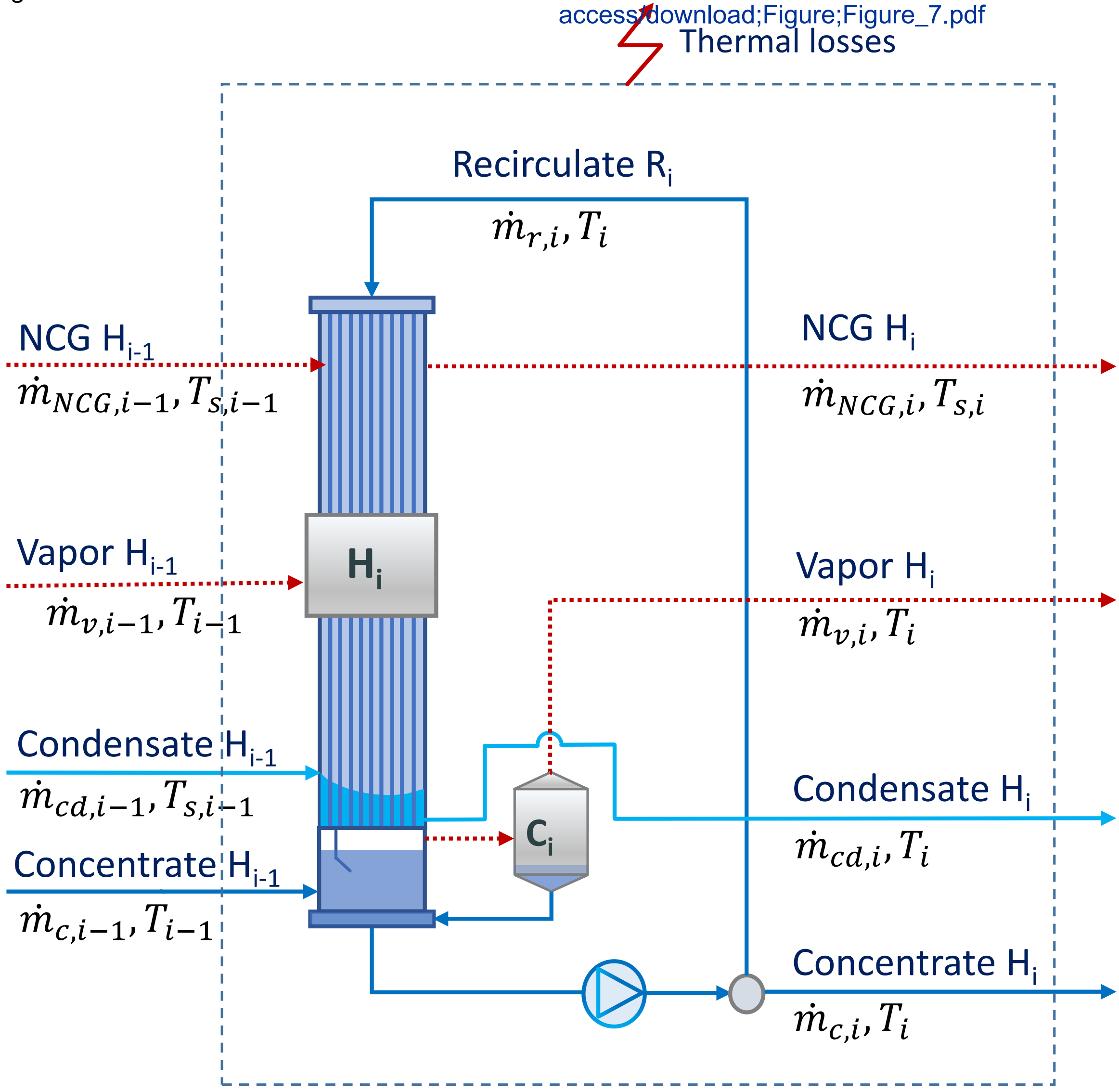
Thermal losses
Recirculate R_i
$\dot{m}_{r,i}, T_i$
NCG H_{i-1}
$\dot{m}_{NCG,i-1}, T_{s,i-1}$
NCG H_i
$\dot{m}_{NCG,i}, T_{s,i}$
H_i
Vapor H_{i-1}
$\dot{m}_{v,i-1}, T_{i-1}$
Vapor H_i
$\dot{m}_{v,i}, T_i$
Condensate H_{i-1}
$\dot{m}_{cd,i-1}, T_{s,i-1}$
C_i
Condensate H_i
$\dot{m}_{cd,i}, T_i$
Concentrate H_{i-1}
$\dot{m}_{c,i-1}, T_{i-1}$
Concentrate H_i
$\dot{m}_{c,i}, T_i$

Figure

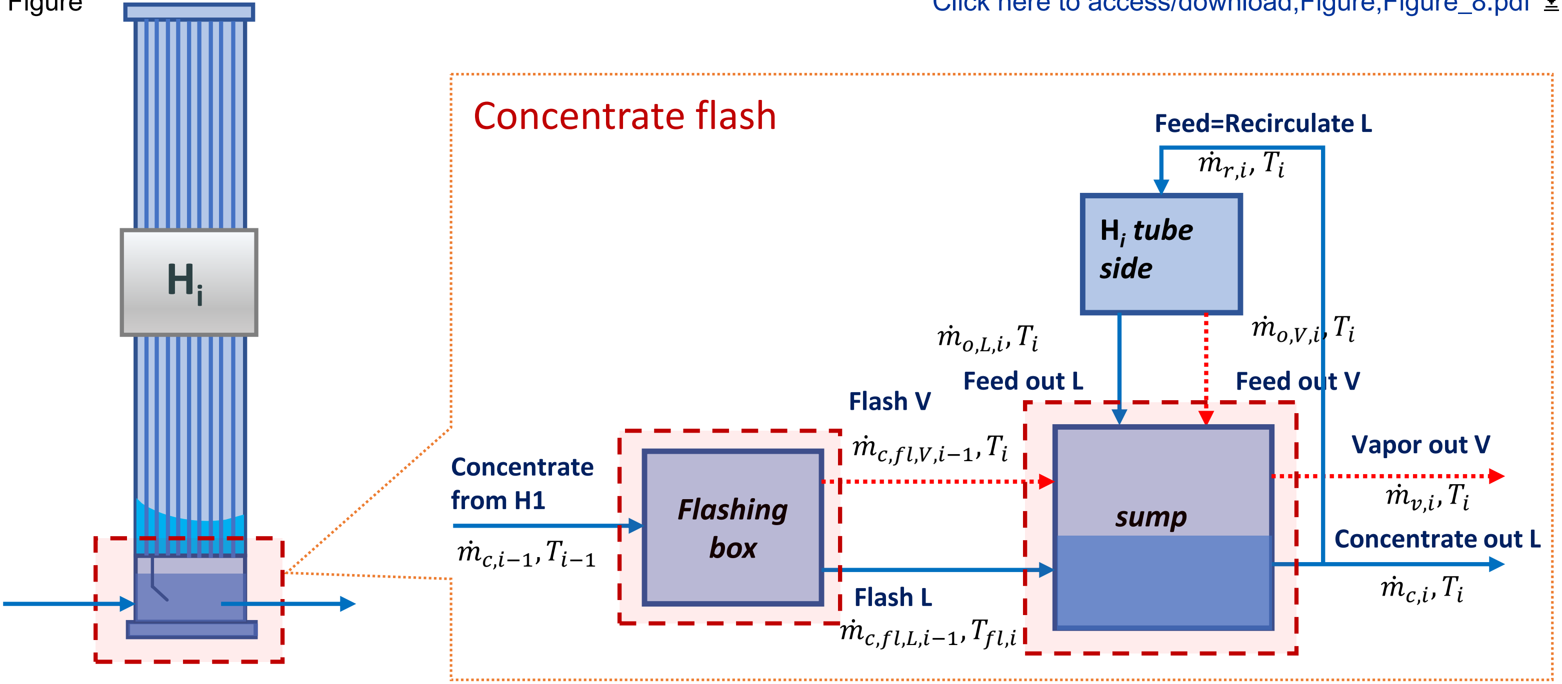

H_i
Concentrate flash
Feed=Recirculate L
$\dot{m}_{r,i}, T_i$
H_i tube side
$\dot{m}_{o,L,i}, T_i$
$\dot{m}_{o,V,i}, T_i$
Feed out L
Feed out V
Flash V
$\dot{m}_{c,fl,V,i-1}, T_i$
Vapor out V
Concentrate from H1
Flashing box
sump
$\dot{m}_{v,i}, T_i$
Concentrate out L
$\dot{m}_{c,i-1}, T_{i-1}$
Flash L
$\dot{m}_{c,i}, T_i$
$\dot{m}_{c,fl,L,i-1}, T_{fl,i}$

Figure

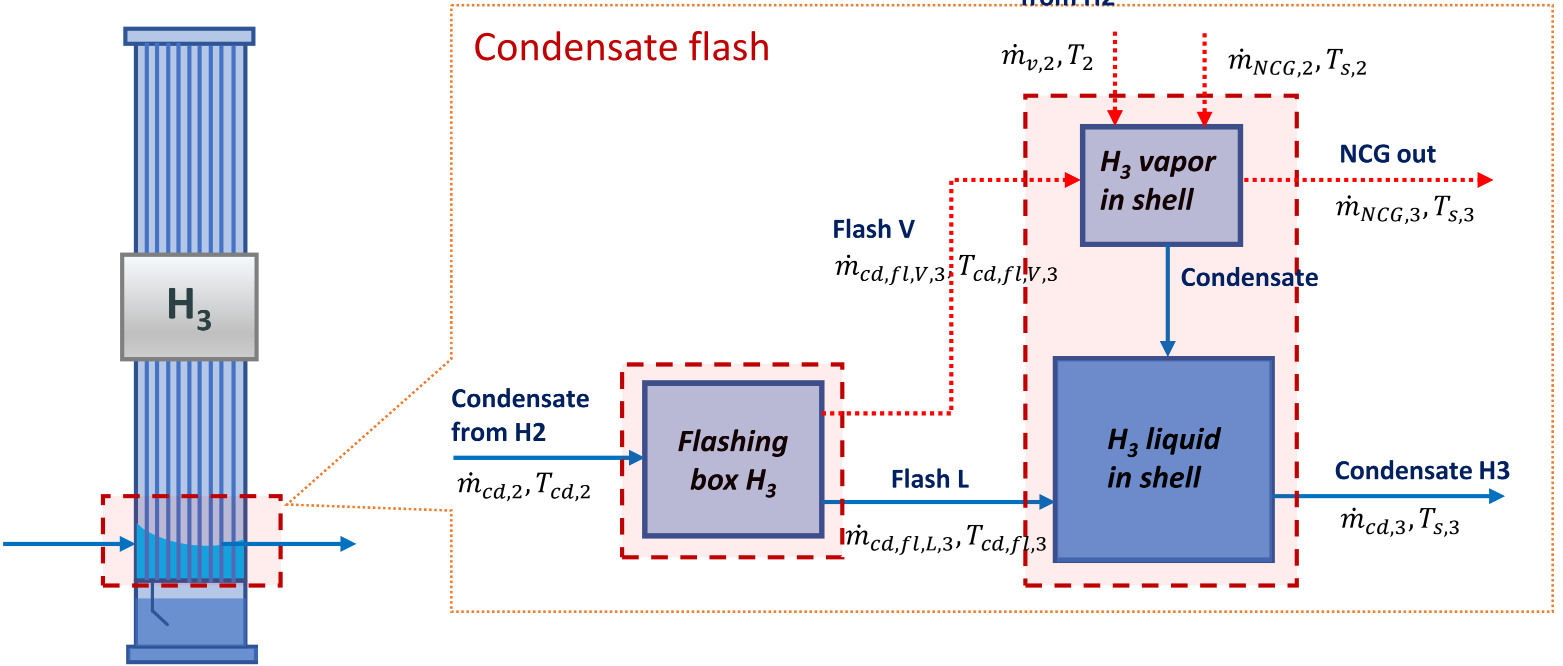
Heating steam from H2
NCG in
Condensate flash
$\dot{m}_{v,2}, T_2$
$\dot{m}_{NCG,2}, T_{s,2}$
H_3 vapor in shell
NCG out
$\dot{m}_{NCG,3}, T_{s,3}$
Flash V
$\dot{m}_{cd,fl,V,3}, T_{cd,fl,V,3}$
Condensate
H_3
Condensate from H2
$\dot{m}_{cd,2}, T_{cd,2}$
Flashing box H_3
Flash L
$\dot{m}_{cd,fl,L,3}, T_{cd,fl,3}$
H_3 liquid in shell
Condensate H3
$\dot{m}_{cd,3}, T_{s,3}$

Figure

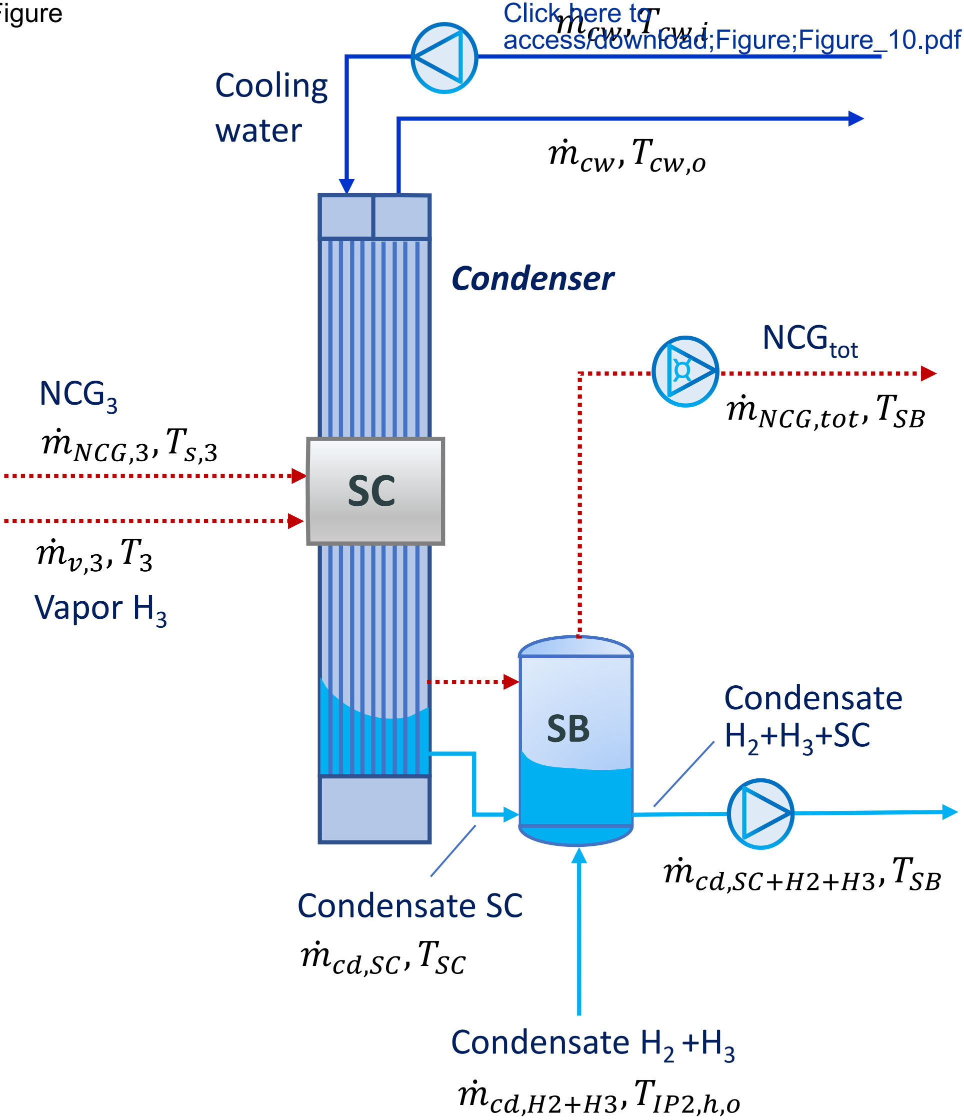

$\dot{m}_{cw}, T_{cw,i}$
Cooling water
$\dot{m}_{cw}, T_{cw,o}$
Condenser
NCG$_{tot}$
$\dot{m}_{NCG,tot}, T_{SB}$
NCG$_3$
$\dot{m}_{NCG,3}, T_{s,3}$
SC
$\dot{m}_{v,3}, T_3$
Vapor H$_3$
SB
Condensate H$_2$+H$_3$+SC
$\dot{m}_{cd,SC+H2+H3}, T_{SB}$
Condensate SC
$\dot{m}_{cd,SC}, T_{SC}$
Condensate H$_2$ +H$_3$
$\dot{m}_{cd,H2+H3}, T_{IP2,h,o}$

Figure

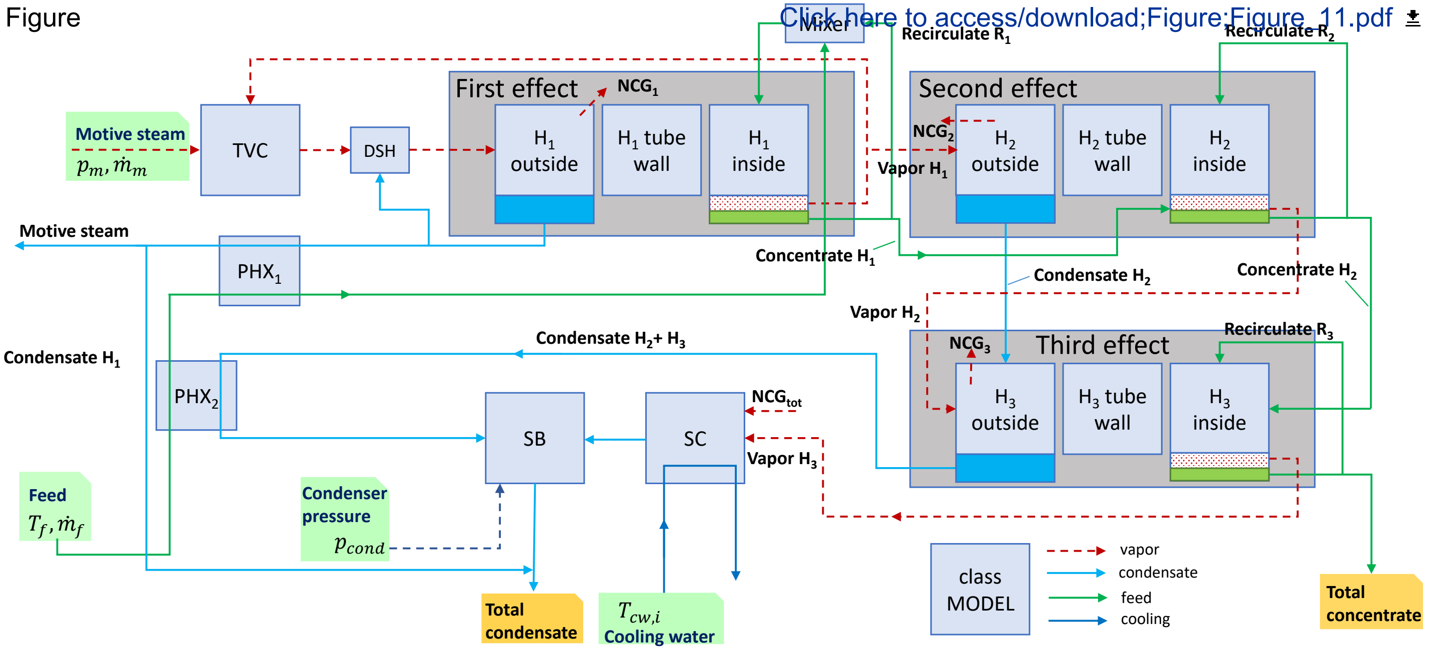

Mixer
Recirculate R_1
Recirculate R_2
First effect
NCG_1
Second effect
Motive steam
$p_m, \dot{m}_m$
TVC
DSH
H_1 outside
H_1 tube wall
H_1 inside
NCG_2
H_2 outside
H_2 tube wall
H_2 inside
Vapor H_1
Motive steam
PHX_1
Concentrate H_1
Condensate H_2
Concentrate H_2
Vapor H_2
Condensate H_2+ H_3
Recirculate R_3
Condensate H_1
PHX_2
NCG_3
Third effect
NCG_{tot}
SB
SC
H_3 outside
H_3 tube wall
H_3 inside
Vapor H_3
Feed
$T_f, \dot{m}_f$
Condenser pressure
p_{cond}
class MODEL
vapor
condensate
feed
cooling
Total concentrate
Total condensate
$T_{cw,i}$
Cooling water

Figure

Click here to access/download;Figure;Figure_12.pdf

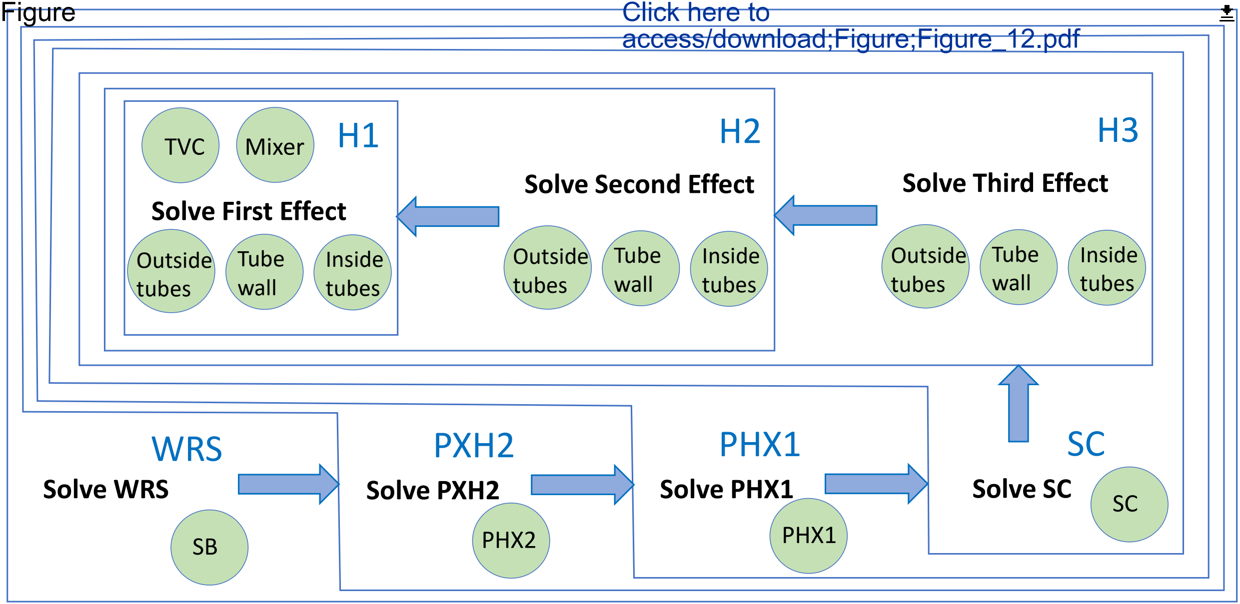

Figure

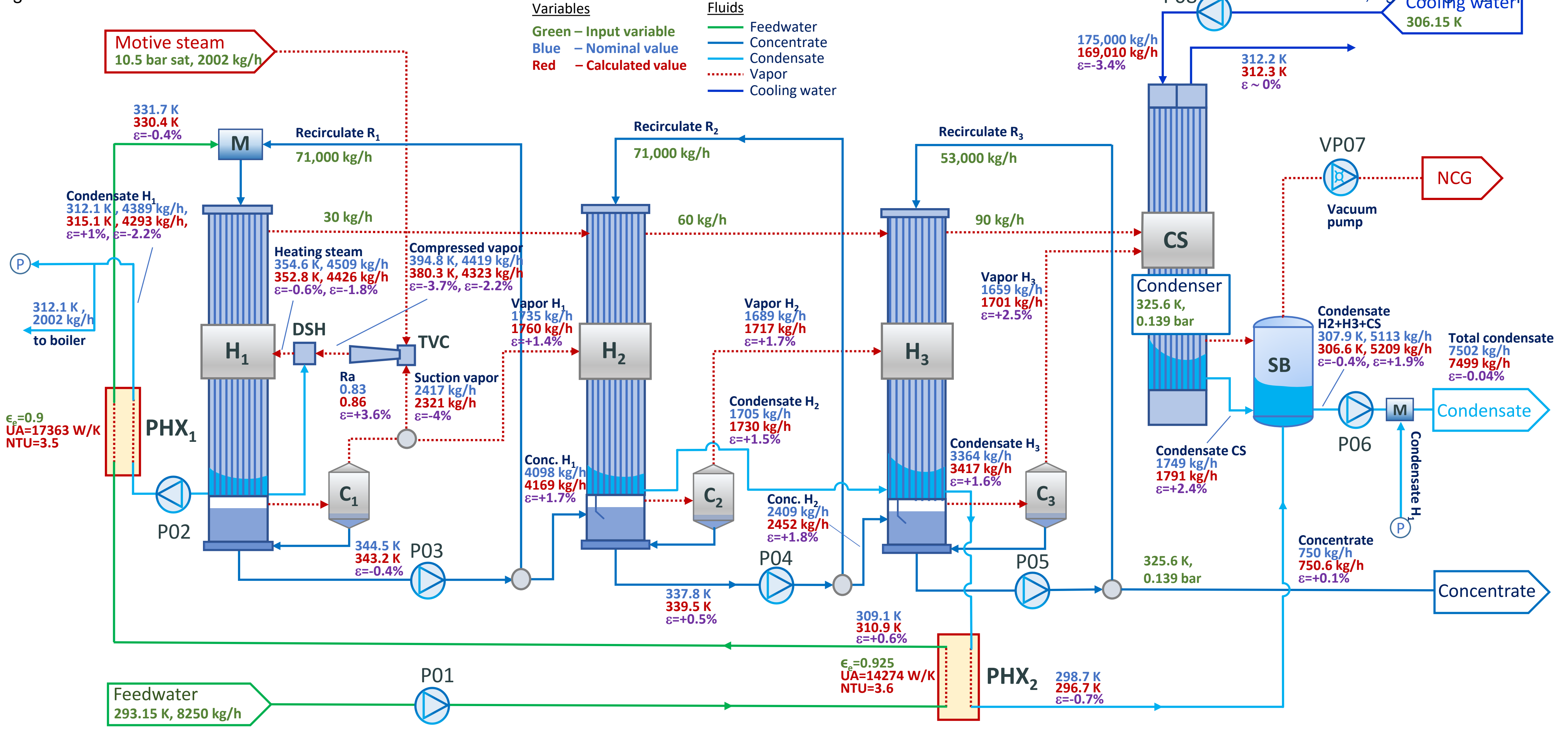

Variables
Green – Input variable
Blue – Nominal value
Red – Calculated value
Fluids
Feedwater
Concentrate
Condensate
Vapor
Cooling water
Motive steam
10.5 bar sat, 2002 kg/h
P08
Cooling water
306.15 K
175,000 kg/h
169,010 kg/h
ε=-3.4%
312.2 K
312.3 K
ε ~ 0%
331.7 K
330.4 K
ε=-0.4%
M
Recirculate R1
71,000 kg/h
Recirculate R2
71,000 kg/h
Recirculate R3
53,000 kg/h
VP07
NCG
Vacuum pump
Condensate H1
312.1 K, 4389 kg/h,
315.1 K, 4293 kg/h,
ε=+1%, ε=-2.2%
30 kg/h
60 kg/h
90 kg/h
CS
Condenser
325.6 K,
0.139 bar
Heating steam
354.6 K, 4509 kg/h
352.8 K, 4426 kg/h
ε=-0.6%, ε=-1.8%
Compressed vapor
394.8 K, 4419 kg/h
380.3 K, 4323 kg/h
ε=-3.7%, ε=-2.2%
P
312.1 K ,
2002 kg/h
to boiler
Vapor H1
1735 kg/h
1760 kg/h
ε=+1.4%
Vapor H2
1689 kg/h
1717 kg/h
ε=+1.7%
Vapor H3
1659 kg/h
1701 kg/h
ε=+2.5%
H1
DSH
TVC
H2
H3
SB
Condensate
H2+H3+CS
307.9 K, 5113 kg/h
306.6 K, 5209 kg/h
ε=-0.4%, ε=+1.9%
Total condensate
7502 kg/h
7499 kg/h
ε=-0.04%
Ra
0.83
0.86
ε=+3.6%
Suction vapor
2417 kg/h
2321 kg/h
ε=-4%
εe=0.9
UA=17363 W/K
NTU=3.5
PHX1
Condensate H2
1705 kg/h
1730 kg/h
ε=+1.5%
Condensate H3
3364 kg/h
3417 kg/h
ε=+1.6%
P06
Condensate
Condensate CS
1749 kg/h
1791 kg/h
ε=+2.4%
Condensate H1
Conc. H1
4098 kg/h
4169 kg/h
ε=+1.7%
C1
C2
C3
Conc. H2
2409 kg/h
2452 kg/h
ε=+1.8%
P02
344.5 K
343.2 K
ε=-0.4%
P03
P04
P05
325.6 K,
0.139 bar
Concentrate
750 kg/h
750.6 kg/h
ε=+0.1%
Concentrate
337.8 K
339.5 K
ε=+0.5%
309.1 K
310.9 K
ε=+0.6%
εe=0.925
UA=14274 W/K
NTU=3.6
PHX2
298.7 K
296.7 K
ε=-0.7%
P01
Feedwater
293.15 K, 8250 kg/h

Figure

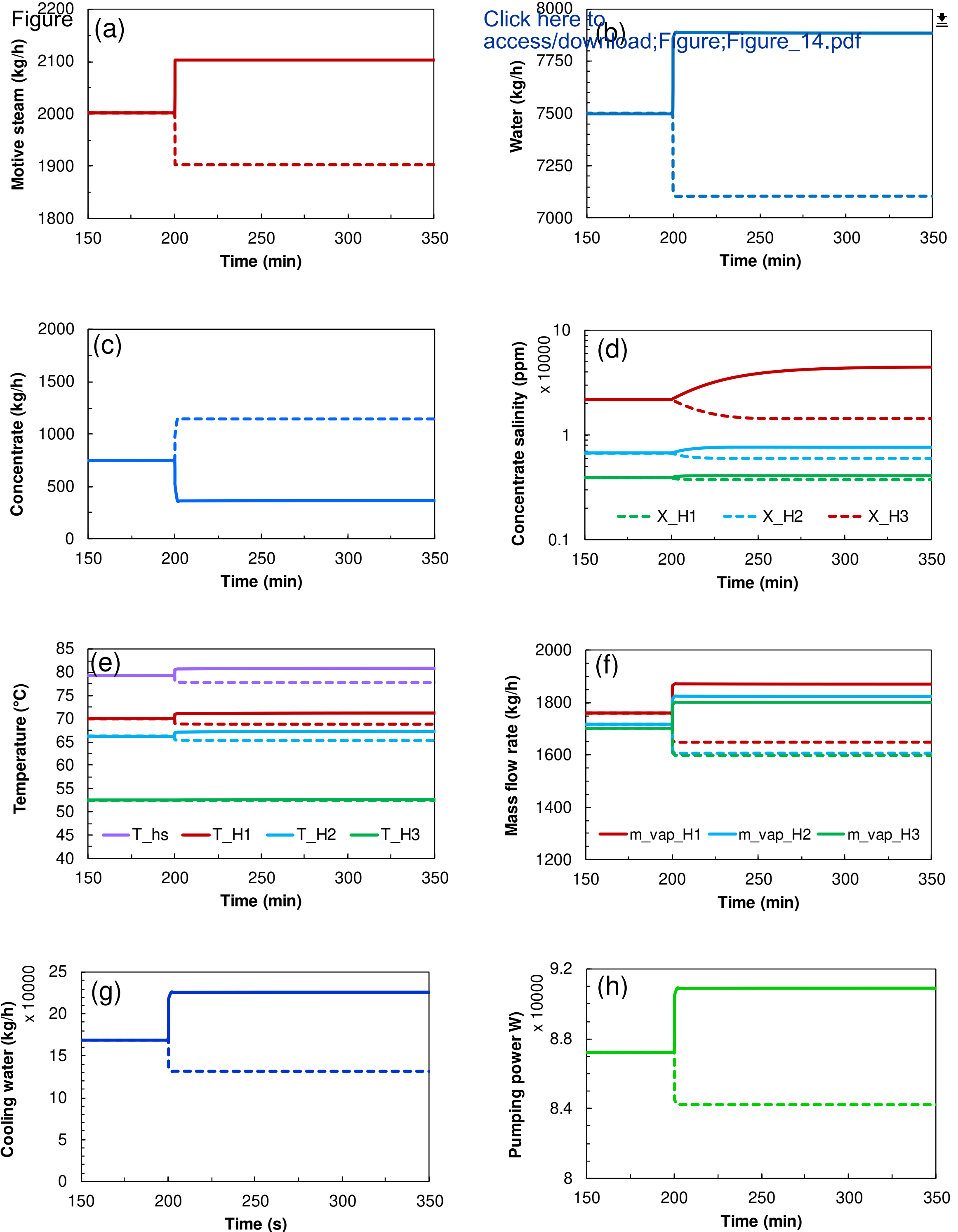
(a)
Motive steam (kg/h)
2200
2100
2000
1900
1800
150 200 250 300 350
Time (min)
(b)
Water (kg/h)
8000
7750
7500
7250
7000
150 200 250 300 350
Time (min)
(c)
Concentrate (kg/h)
2000
1500
1000
500
0
150 200 250 300 350
Time (min)
(d)
Concentrate salinity (ppm)
x 10000
10
1
0.1
X_H1
X_H2
X_H3
150 200 250 300 350
Time (min)
(e)
Temperature (°C)
85 80 75 70 65 60 55 50 45 40
T_hs
T_H1
T_H2
T_H3
150 200 250 300 350
Time (min)
(f)
Mass flow rate (kg/h)
2000 1800 1600 1400 1200
m_vap_H1
m_vap_H2
m_vap_H3
150 200 250 300 350
Time (min)
(g)
Cooling water (kg/h)
x 10000
25 20 15 10 5 0
150 200 250 300 350
Time (s)
(h)
Pumping power W)
x 10000
9.2 8.8 8.4 8
150 200 250 300 350
Time (min)

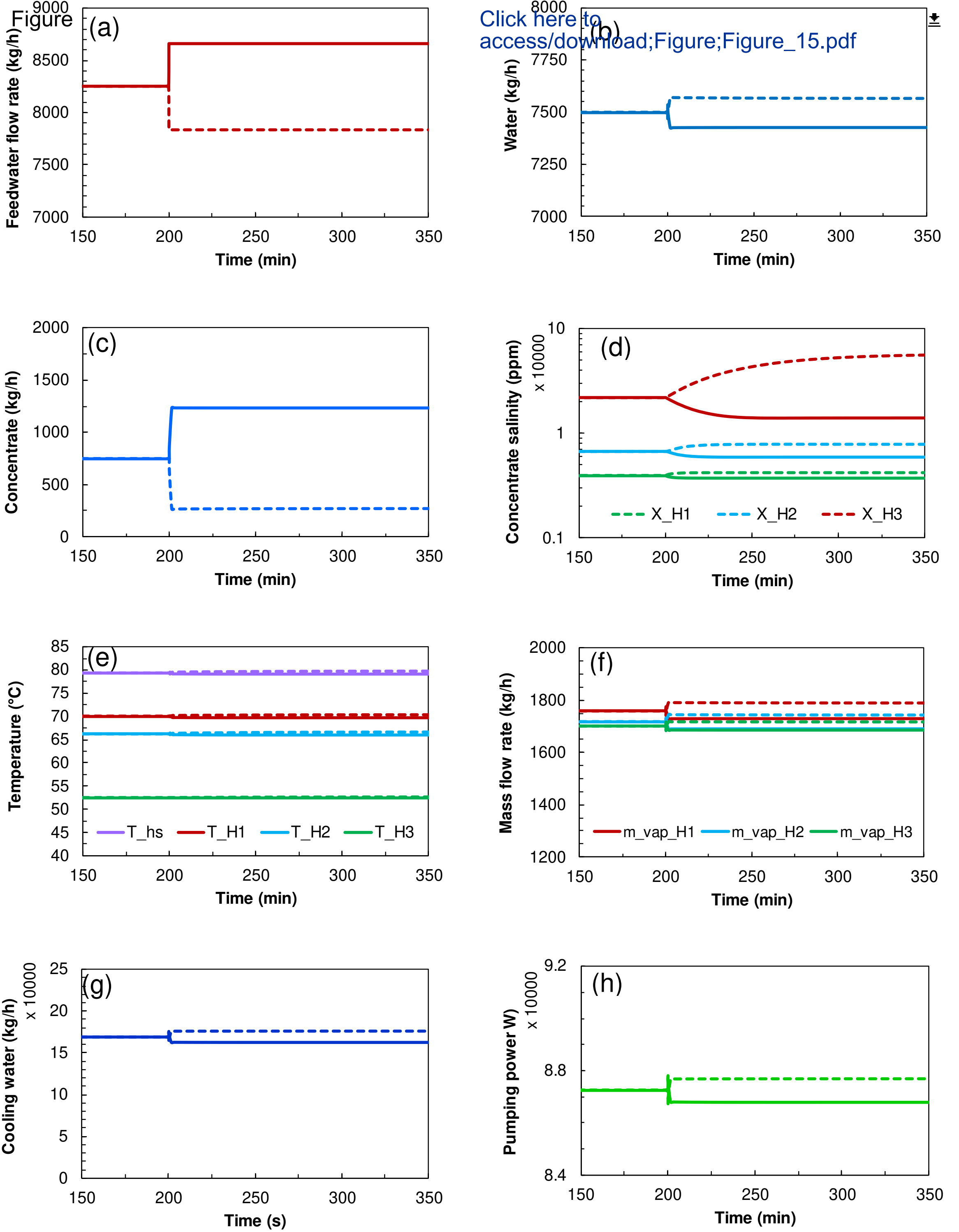
(a)
Feedwater flow rate (kg/h)
Time (min)
(b)
Water (kg/h)
Time (min)
(c)
Concentrate (kg/h)
Time (min)
(d)
Concentrate salinity (ppm)
x 10000
X_H1
X_H2
X_H3
Time (min)
(e)
Temperature (°C)
T_hs
T_H1
T_H2
T_H3
Time (min)
(f)
Mass flow rate (kg/h)
m_vap_H1
m_vap_H2
m_vap_H3
Time (min)
(g)
Cooling water (kg/h)
x 10000
Time (s)
(h)
Pumping power W)
x 10000
Time (min)

Figure

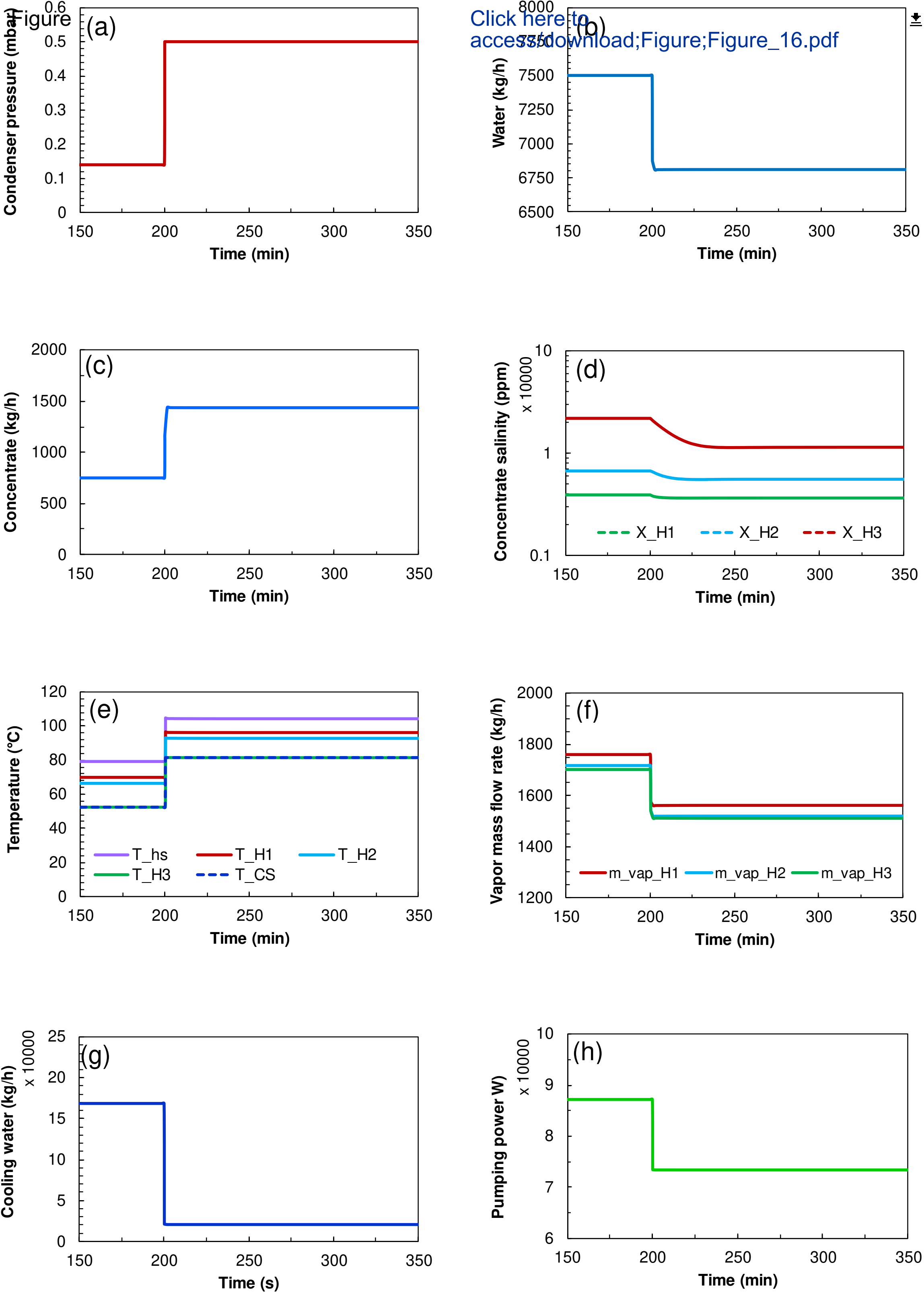
(a)
Condenser pressure (mbar)
Time (min)
(b)
Water (kg/h)
Time (min)
(c)
Concentrate (kg/h)
Time (min)
(d)
Concentrate salinity (ppm)
x 10000
X_H1
X_H2
X_H3
Time (min)
(e)
Temperature (°C)
T_hs
T_H1
T_H2
T_H3
T_CS
Time (min)
(f)
Vapor mass flow rate (kg/h)
m_vap_H1
m_vap_H2
m_vap_H3
Time (min)
(g)
Cooling water (kg/h)
x 10000
Time (s)
(h)
Pumping power W)
x 10000
Time (min)

Figure

Click here to access/download;Figure;Figure_17.pdf

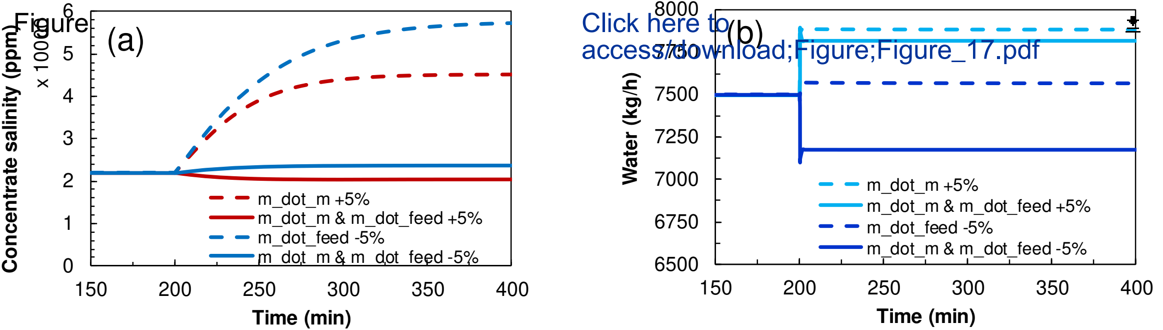

Declaration of interests

☒The authors declare that they have no known competing financial interests or personal relationships that could have appeared to influence the work reported in this paper.

☐The authors declare the following financial interests/personal relationships which may be considered as potential competing interests: